The Design and Construction of a Flying Bird Robot

done by **Marius Bensch**

supervised by **Professor Johnathan Tapson**

and co-supervised by **Mr. Stephen Marais**

Thesis prepared in fulfilment of the requirements of a Master of Science in Electrical Engineering at the University of Cape Town

Acknowledgments

Thanks are due to:

- Professor Jonathan Tapson for assigning this project to me and assisting me in doing research in an area I find very interesting.
- Mr. Stephen Marais, who has had admirably guided an electrical engineering undergraduate through what turned out to be a project with a high mechanical content.
- Mr. Glen Newins and the entire workshop staff for their help with parts.
- Dr. Robert Simmons for an interesting discussion.
- Mr. Hubert Tomlinson for his help with the wind tunnel.
- Mr. Chris Wozniak for his help with the laser cutting machine.
- Mrs. Denise Hamerton and Mr. Vincent Bartnick of the South African Museum (Iziko) for the opportunity to dissect a Cape Vulture specimen.
- Thorsten Klingelhoeffer for his second pair of hands during the dissection at Iziko.
- Peter Henson for his assistance with a software issue or two.

1 Declaration

I declare that this thesis is my own unaided work. I believe that all information drawn from other sources has been referenced.

I have used the IEEE convention for citation and referencing. Each significant contribution to this thesis from the work of other people has been cited and referenced.

The submission of this thesis is in partial fulfilment of the requirements for the degree of Master of Science in Electrical Engineering at the University of Cape Town.

In addition, I also declare that this thesis has not been submitted before for any degree or examination at this or any other University.

Signature.....

December 2010

2 Design Brief

Investigation into the Design and Construction of a Flying Bird Robot

Project supervised by Professor Jonathan Tapson and co-supervised by Mr. Stephen Marais

The purpose of this project is to investigate the issues surrounding the design and construction of a flying bird robot. The ideal would be to re-create a model of a bird that looks like bird, functions like a bird with regard to the biomechanical issues involved in flight and uses control systems that emulate the ones used by the bird to control the flight path.

The project may be summarised as follows:

- Introduction of concepts that are relevant to the discussion
- Investigation into what has been done before and how relevant problems were overcome or mitigated
- Descriptions and results surrounding the dissection of a Cape Vulture
- Conduction of an experiment delving into the effects of tail motion
- Drawing of overall conclusions and recommendations

Table of Contents

List of Figures

Glossary of Terms

L.E.	Leading Edge
T.E.	Trailing Edge
A.O.A.	Angle of Attack
Z.L.A.	Zero Lift Angle
A.C.	Aerodynamic Centre
C.G.	Centre of Gravity

1 Introduction

The concept of flight holds a particular fascination for many people. The idea of escaping the force of gravity and leaving behind what holds one down implies a freedom that few other things can.

Since ancient times the dream of flying has found a niche in man's consciousness, as evidenced by myths and legends such as that of Daedalus and Icarus [1], but not until a little over a hundred years ago had technology advanced sufficiently for the first powered flight of a 'heavier-than-air' craft to come to pass in the form of the Wright brothers' historical event at Kitty Hawk in 1903 [2]. Aeronautics has enjoyed an exceptional development since that time, and to date there are many genres of aircraft, from jets to airliners and sailplanes to hang gliders, but no man-made machine seems to be able to synthesise efficiency, an essential simplicity, elegance and certain performance parameters in the way that birds do. In a sense birds remain the *de facto* standard for all things flying, and although first attempts at flying were directly inspired by birds, the machines that have developed from this are no longer bird-like. Birds, for example, do not have hinged control surfaces such as a rudder for steering. The Wright brothers' machine "for all practical purposes ended the use of birds as models for aircraft design" [3]. However, there seems to be "a growing number of aircraft designers who wish to go back to the bird model" [3] for a number of different reasons.

The aim of this project is to look at the challenges that arise in building a remotely controllable flying bird. The idea is not simply to build a model aircraft along conventional lines and then give it a 'shell' that looks bird-like, but to emulate shapes and movable joints or surfaces relevant to flight dynamics as closely as possible.

The report starts with an introduction to some relevant background theory. Basic bird terminology is covered to ease the following discussions. Aerodynamic concepts and terminology are covered slightly more in-depth since this is necessary to grasp the fundamental problems involved in getting any 'heavier-than-air' craft to remain airborne, let alone one with a predefined, in this case bird-like, shape and with some minimum demands with regard to stability and controllability in the air.

The next chapter introduces some of the models that have already tackled these challenges. Many projects that emulate flying animals have already been undertaken. Birds, pterosaurs and even insects have been modelled and these models flown. Most of these designs involve some compromise in at least one aspect of the design and are in general 'conventional' designs that have been made to look like a bird. However, they all tackle at least one of the difficulties inherent to creating a bird-like flying model and the solutions that they implement will be investigated since they are clearly a resource for any further developments.

During the course of this research the South African Museum (Iziko) was approached for the possibility of dissecting a large raptor and the opportunity to study and dissect a Cape Vulture specimen yielded some very interesting results. Their discussion forms a part of this chapter, and any modelling done in this project is based on the Cape Vulture.

It will become clear during the reading of this document that the complete construction of a flying bird model is not feasible in the given context. A decision that was made was that the scope of this project would be limited to investigating the effect of various tail positions on the flight path, and the next chapter focuses on an experiment that was undertaken particularly for inclusion into this document. The mechanical components that formed part of the experiment are described, followed by an account of the actual experiment. The data that was collected is then analysed and conclusions are drawn.

It is hoped that the work presented here can assist in any future efforts to create a flying bird model.

2 Literature Review and Relevant Background Theory

2.1 Chapter Introduction

This chapter forms a basic introduction to some key terminology and concepts with regard to birds and aerodynamics. Familiarity with these items will enable the reader to understand the challenges involved in the construction of a flying bird robot.

To begin, some terms describing the physiology of birds are introduced. Then some aerodynamic concepts are explained. Following this some of the problems involved in implementing these concepts in a bird-like structure are investigated. Projects that have been undertaken by others are showcased and the methods used to deal with relevant problems described, also showing how various trade-offs have to be made. Finally, the results of the dissection of a Cape Vulture are discussed, in particular with regard to the primary feathers.

2.2 Introduction to Bird Terminology

The following paragraphs are intended to give the reader an overview of terms relevant to this project with regard to birds.

Flight feathers are those feathers that create the surfaces required for flight, as opposed to other feathers such as the down feathers whose main function is the conservation of body heat. The flight feathers of the wing are called remiges (singular 'remex', from the Latin word for 'oarsman') whereas those of the tail are called retrices (singular 'retrix', from the Latin word for 'helmsman').

The reader is referred to figure 2.1 overleaf for the following explanation. The remiges are divided into primaries, secondaries and tertials. The primaries are those feathers that are attached to the hand of the bird, i.e. from the wrist joint outwards. The secondaries are attached to the ulna, i.e. from the elbow to the wrist. The tertials are attached to the humerus, i.e. from the shoulder to the elbow. The tertials are not shown in the figure; it was used nevertheless since this was considered an instructive figure showing both feathers and some skeletal structure. There are various numbering conventions with different advantages depending on the ornithological context such as moult processes or body structure. In this project the following convention is adopted:

- Primaries are prefixed with the letter 'P'.

- Secondaries are prefixed with the letter ‘S’.
- Tertials are prefixed with the letter ‘T’.

Numbering starts at the tip and ascends as the body is approximated. The count restarts when moving from the primaries to the secondaries, but not when moving from the secondaries to the tertials. Thus in moving from the tip towards the body the outermost primary is P1, the innermost primary may be P10, the first secondary is S1, the last may be S11, the first tertial would then be T12, and the last might be T17.

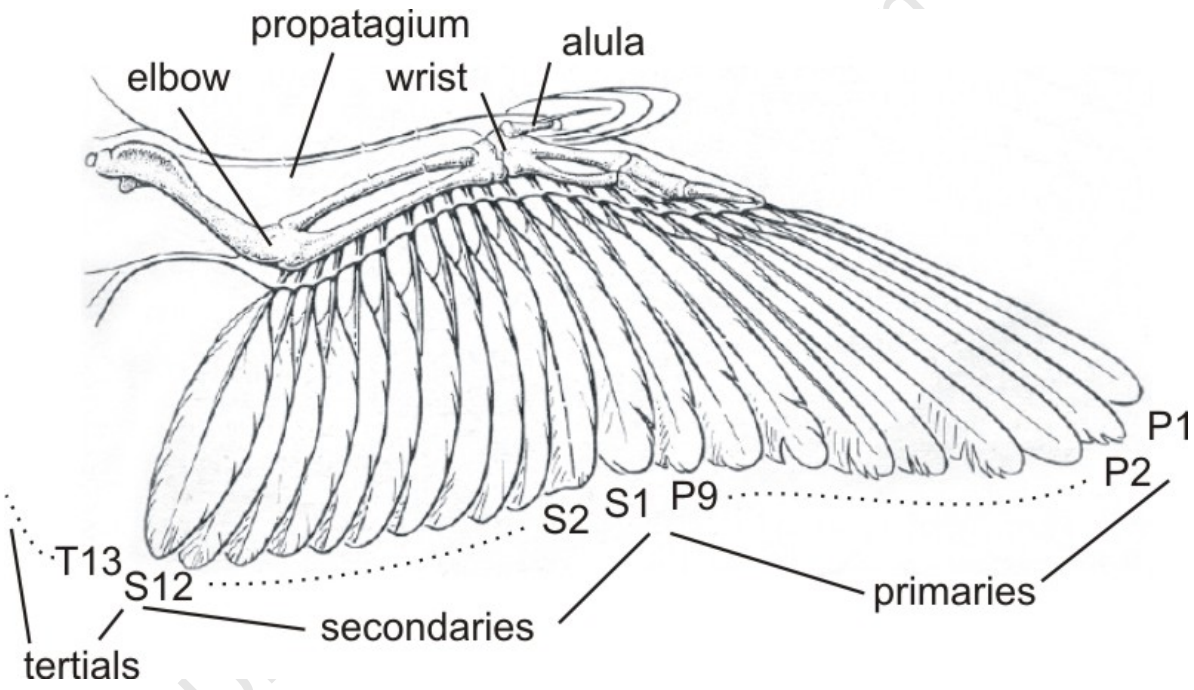

Figure 2.1: Basic relevant Bird Wing Terminology (edited from [4])

For the terminology with regard to flight feathers figure 2.2 may be referred to.

A flight feather consists of a main shaft called the ‘rachis’ and the ‘vane’ that forms the surface of the feather. For most primaries the front part of the vane is considerably smaller in area than the back part, whereas in other feathers the areas are more evenly distributed. The bottom part of the rachis is known as the calamus and actually reaches a short distance into the vaned part of the rachis.

The vanes of the primary feathers of many large soaring birds become narrower towards the tip at a fairly distinct part along the rachis. These are ‘emarginations’. ‘Notch’ refers to the more sudden change in width that may only found on the back part of the vane.

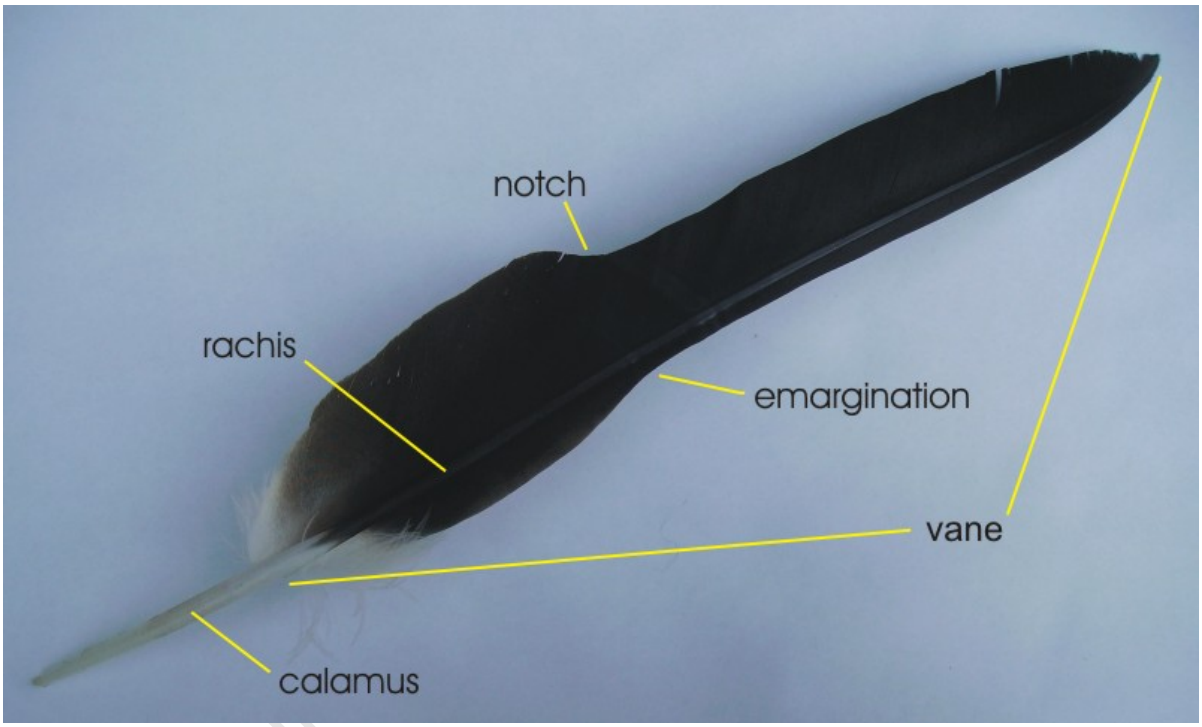

Figure 2.2: Basic Feather Terminology

2.3 Introduction to Aerodynamic Terminology / Concepts

Aerodynamics plays an important role in this project and the relevant terms and background knowledge are introduced in the following paragraphs. Most of the information comes from [5] and [6].

2.3.1 The Roll, Pitch and Yaw Axes

The roll, pitch and yaw axes are simply reference axes to describe the motion of an aircraft and are depicted in figure 2.3. Pitching upwards or yawing to left refer to the front of the aircraft moving up or to the left respectively. In rolling to the left the left wingtip (as viewed from behind) drops.

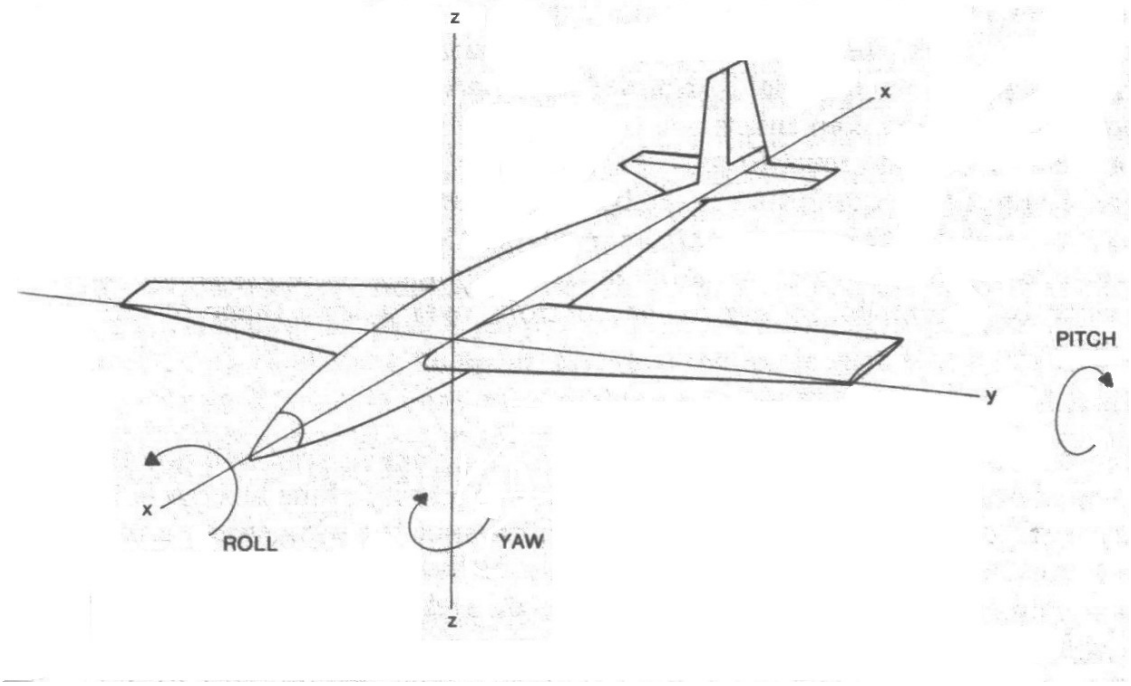

Figure 2.3: Roll, Pitch and Yaw Axes [5:161]

2.3.2 Chord, Camber and Thickness, Leading Edge and Trailing Edge

A description of how an airfoil is generated will clarify the terms chord, camber and thickness, and figure 2.4 from [6] may be referred to.

Using a two-dimensional x-y coordinate system a line is drawn from (0, 0) to (1, 0). This is the 'chord' of the airfoil. When the airfoil is scaled and applied to an actual wing the chord is the distance from the 'leading (front) edge' (L.E.) of the wing to the 'trailing (back) edge' (T.E.) of the wing. A curved line (some polynomial $y = f(x)$) starting at (0, 0) and terminating at (1, 0) is drawn. This is the 'camber line' (labelled as its alternative name 'Mean line' in the figure). Typically the first derivative of said polynomial is positive at (0, 0), becomes zero at some point and ends negative at (1, 0). The camber of the resulting airfoil is the maximum value of $f(x)$ in the range x = [0, 1] and is typically expressed as a percentage of the chord.

A symmetrical thickness distribution (symmetrical about the chord line), which is described by a series of x-y coordinates at a variable number of x values, is chosen. The maximum value of this thickness distribution is the 'thickness' of the resulting airfoil. This thickness distribution is then superposed on or wrapped around the mean line (using the equations for x_U, y_U, x_L and y_L), resulting in the desired airfoil.

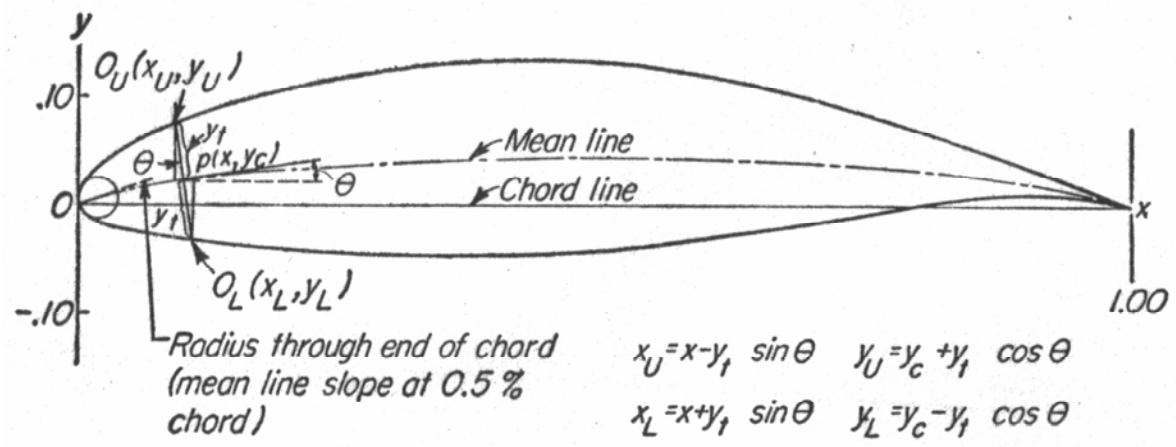

Figure 2.4: Airfoil Geometry [6:112]

2.3.3 Angle of Attack, Zero Lift Angle, Aerodynamic Centre and Pitching Moment Coefficient

With reference to figure 2.5, the 'geometric angle of attack' (A.O.A.) is simply the angle between the chord line and the air stream that the airfoil finds itself in. Typically, the airfoil is still generating lift when the A.O.A. is zero. At some negative angle known as the 'zero lift angle' (Z.L.A.), the lift becomes zero. This is the reference angle for the 'aerodynamic angle of attack'. If not specified it is assumed that angle of attack refers to the geometric angle of attack.

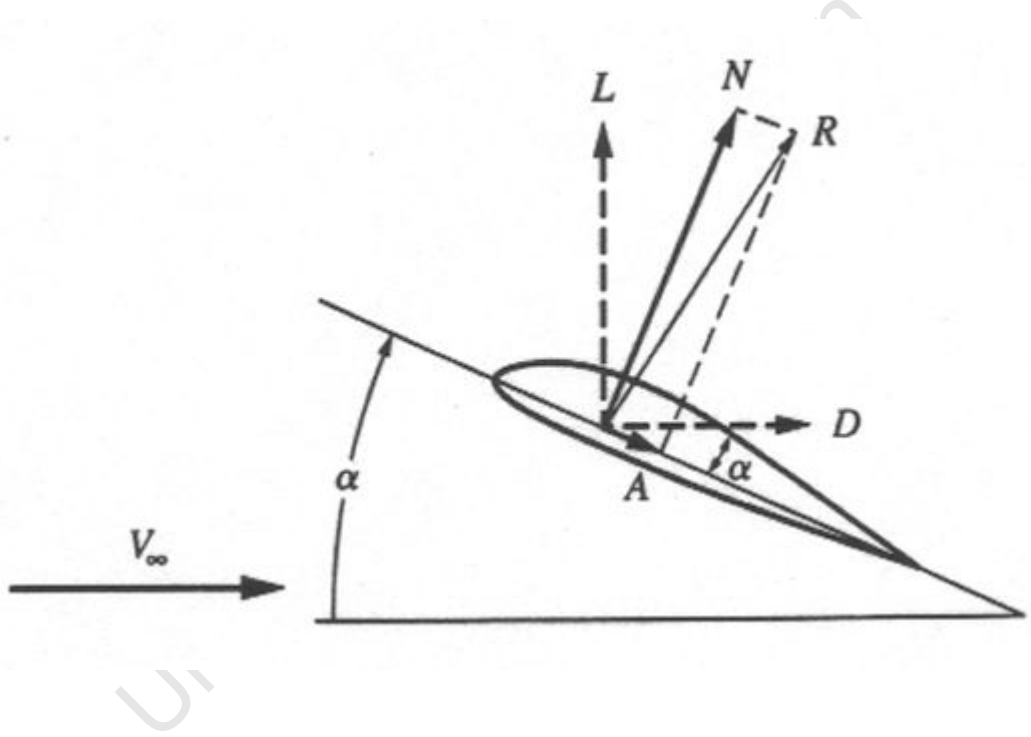

Figure 2.5: Figure showing Definition of Angle of Attack [7]

Assume a positive aerodynamic angle of attack for this discussion.

As the air stream moves around the airfoil the laws of physics (Bernoulli's principle) dictate that a force is generated, since the airflow is forced to follow the shape of the wing, which generates a region of increased pressure beneath the wing and a region of decreased pressure above it. This is typically resolved into 'lift' (that component of the force that is perpendicular to the air stream) and 'drag' (that component of the force that is parallel to the air stream). For graphing and comparison purposes these forces are reduced to coefficient form c_l and c_d, using the equations in appendix A. A convention that is not always observed

is to use uppercase letters (e.g. C_L) when referring to a whole plane or wing and lowercase letters (e.g. c_l) when referring to the airfoil section alone. The two differ since a wind tunnel eliminates some detrimental effects on performance. If the A.O.A. is too large in either the negative or positive direction the air stream cannot flow 'smoothly' around the airfoil, vortices are generated and lift decreases and drag increases markedly. This condition is known as the 'stall'.

As the air stream moves around the airfoil the generated force also tends to rotate the airfoil, thereby changing the A.O.A. As for lift and drag, this force is reduced to the 'pitching moment coefficient' c_{mo} (see Eqn. 7). The magnitude of this force varies with A.O.A. when measured at arbitrary points along the chord, but when measured at 25% it is found to be constant (or nearly so) within the range of angles of attack in which the airfoil does not stall. The 'aerodynamic centre' (A.C.) is that point on the wing at which the c_{mo} is considered constant and also the point through which the lift and drag forces are considered to act.

In the general case the c_{mo} is negative, the airfoil is unstable in the pitch axis and the A.O.A. will not be maintained unless another force (such as that supplied by a tailplane) is applied.

2.3.4 Wingtip Vortices

Wingtip vortices create what is known as 'induced drag'. In general, wingtip vortices account for a large portion of the total drag of an aircraft. Referring to figure 2.6, they come about in the following manner:

When the air pressure is greater beneath the wing than above it, lift is generated as described above. An unavoidable effect that takes place simultaneously is that the air simply spills around the wingtip from the bottom to the top wing surface. Since the wing is moving forward at the same time, spiral-like vortices trail from the wingtips. Figure 2.7 is an impressive demonstration of how much air may be displaced by wingtip vortices.

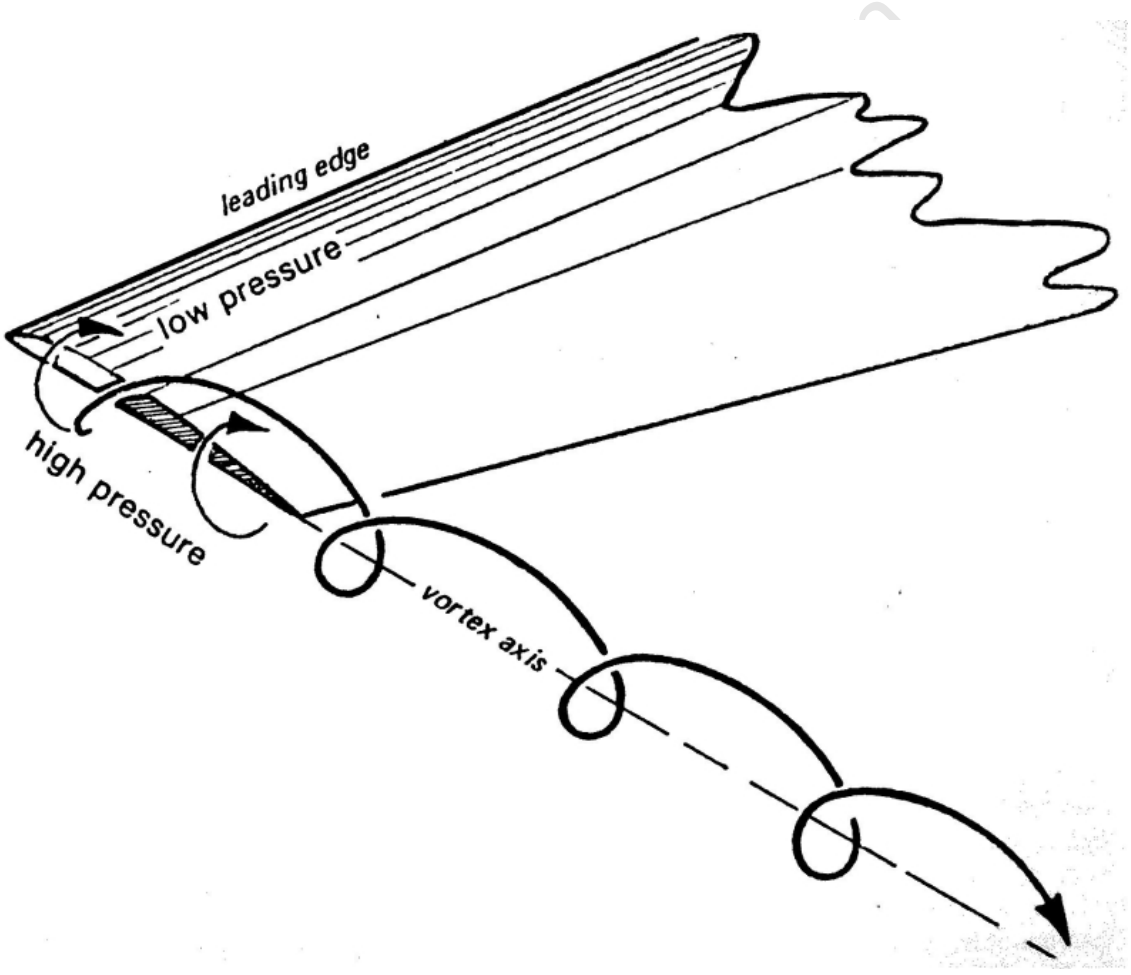

Figure 2.6: Generation of Wingtip Vortices [5:54]

Figure 2.7: An impressive Demonstration of the Effect of Wingtip Vortices [8]. The spiral-like shapes that this smoke bomb has been drawn into are the result of pressure gradients generated around the wingtip.

At low speeds and high c_l, induced drag is relatively large and becomes smaller at higher speeds and lower c_l. At zero lift the induced drag also becomes zero since there is no difference in the air pressures above and below the wing. Conversely, 'form drag' which is simply the resistance of a fluid to any solid body moving through it increases with increasing speed. Adding these two types of drag results in the total drag as shown in figure 2.8 and it may be seen that total drag is at a minimum where induced and form drags are equal.

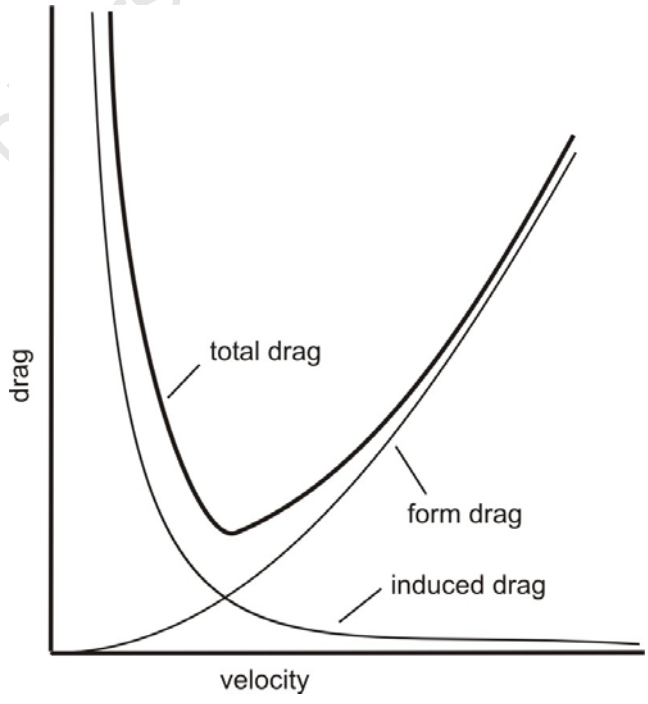

Figure 2.8: Contributions of Induced and Form Drags to Total Drag (redrawn from [5: 29])

2.4 Bird Aerodynamics

As living organisms with a central nervous system and the bio-mechanical capacity to articulate all the pertinent joints of their bodies, birds have overcome the problems associated with controlled flight in ways that are difficult to emulate for the average model builder. Some of these problems are introduced in the following discussion.

2.4.1 The Problem of Pitch Control

As elucidated in section 2.3.3, an airfoil by itself will tend to rotate about its A.C. due to the negative pitching moment and not maintain its angle relative to the airflow unless another force is applied to counter that tendency.

In the general case a horizontal stabiliser some distance behind (or in front of, in the case of a 'canard' configuration) the wing provides that force, as depicted in figure 2.9. Pitch control is then effected by varying the force provided by the horizontal stabiliser, either by changing the A.O.A. of the entire stabiliser ('all flying tailplane') or by creating a hinged surface at the back of the stabiliser (known as an 'elevator') whose deflections change the camber of and thus the force created by the stabiliser. The angular difference between the chord line of the wing and that of the horizontal stabiliser is known as the 'angle of incidence' and is positive if the front wing is at a more positive angle than the rear wing.

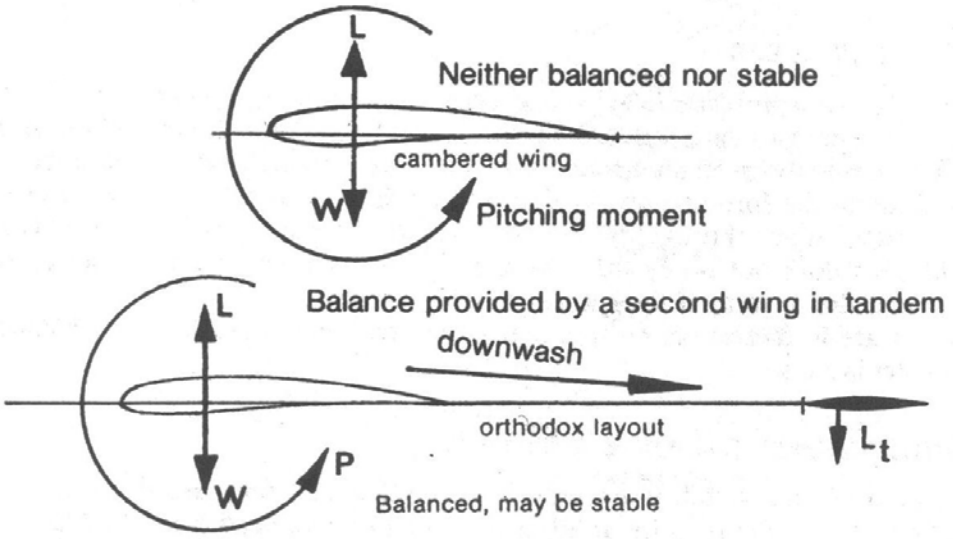

Figure 2.9: Stabilisation of unstable Airfoil by additional Flying Surface [5:162]

In birds, the tail is not primarily used as a pitch control device to sustain a level orientation in flight [9]. The short lever arm between the A.C. of the wing and the A.C. of the tail make it relatively ineffective for the tail to be used for this purpose. Some species in particular, such as the bateleur, have very short stubby tails. The tail is more useful for manoeuvring or increased efficiency in various flight regimes such as slow flight or landing.

Pitch stability is effected by the bird moving the A.C. forwards or backwards with respect to the C.G. [9]. This is achieved by changing the geometry of the wing, i.e. sweeping the wings forwards or backwards. This necessitates some form of pitch sensing and a sufficiently fast control loop (both contained in the bird's biological systems) to control the movement of the wings and the (bio-) mechanical ability to sweep the wings forwards and backwards.

These difficulties generally preclude the use of variable sweep as a means of controlling pitch stability in flying models.

2.4.2 The Problem of Yaw Control

The general solution to obtain stability in the yaw axis is the use of a vertical stabiliser some distance behind the 'neutral point', the A.C. of the aircraft as a whole. Under idealized conditions, and as opposed to the horizontal stabiliser, the vertical stabiliser produces no force other than drag since its airfoil would be symmetrical and its A.O.A. zero. Only when some asymmetry in the airflow arises does the A.O.A. change and the vertical stabiliser produces a corrective force. In the same manner as for the elevator a hinged surface at the back of the vertical stabiliser (known as a 'rudder') may be fitted to change the camber and produce a yawing force.

Aircraft that implement ailerons for control in the roll axis also experience 'adverse yaw', an effect whereby the up-going wingtip is made to produce more lift and therefore more drag (with the opposite effect occurring on the down-going wingtip), thus yawing the aircraft in the direction opposite to that of the roll (yaw left as a result of roll right and vice versa). Figure 2.10 shows the changes in lift and drag distributions as the ailerons are deflected. The rudder may be used to produce a corrective yawing force in the opposite direction.

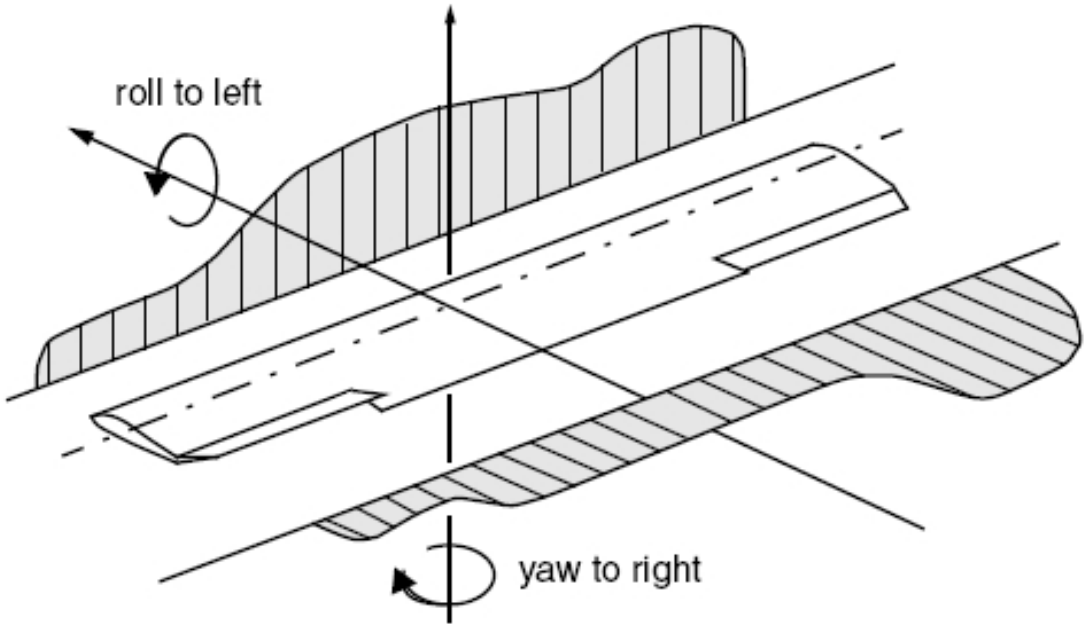

Figure 2.10: The Origin of Adverse Yaw [3:10]

Birds, as is immediately evident, do not have a vertical stabiliser as such and other means need to be made use of to obtain stability in the yaw axis.

Gottfried Sachs shows how slotted wingtips [10] (or sweepback in the outer sections of the wing [11]) and the effects of the tail on the airflow [12] have a positive impact on yaw stability. These are static effects in the sense that they do not require motion of any part of the bird's body.

In contrast to this, a bird is also able to rotate its tail along the roll axis and an up or down motion of the tail then also generates a force that rotates the bird about the yaw axis. This opens up the possibility of using the tail to achieve yaw control around the yaw axis. The experiment that was conducted and that is described in chapter 3 investigates this possibility in more detail.

2.4.3 The Problem of Induced Drag

Nature displays two general solutions for birds to the problem of wingtip vortices.

One is to equip the bird with long, pointed (high aspect ratio) wings, such as those of an albatross (see figure 2.11 overleaf for a graphic comparison of the four different basic wing types in birds). The aspect ratio is given by $A = \frac{b^2}{S}$, where A is the aspect ratio, b is the span and S is the surface area of the wing. With a high aspect ratio wing, the wingtip accounts for a proportionally smaller part of the whole wing and the detrimental effects on performance of the wing are smaller. The induced drag coefficient is given by $C_{Di} = k \times \frac{C_L{}^2}{\pi \times A}$, where k is a factor to allow for deviations from the elliptical lift distribution. The ideal lift distribution is generally thought of as being elliptical in shape, i.e. the middle of the wing provides the most lift per span-wise segment, with the lift decreasing in an elliptical sense towards the tips. The equation shows that doubling the aspect ratio halves the induced drag. In general these birds will also be high speed flyers, which keeps Reynolds numbers up (increasing the efficiency of the airfoil) and keeps the required c_l down, which reduces the drag generated by the wingtip vortices.

The Reynolds number is a quantity from fluid dynamics [6] and is given by $\mathrm{Re} = \frac{\rho V L}{\mu}$, where Re is the Reynolds number, L is the length (wing chord in these discussions), and μ is the viscosity (of air in these discussions). In physical terms the Reynolds number contains factors that compare the speed of the body in question to the speed of the molecules making up the fluid through which it moves and the size of the body to the average free path of the molecules. Lower Reynolds numbers thus make the air behave more 'grainy' whereas higher Reynolds numbers make the air behave more like an ideal fluid.

The other solution is to equip the bird with broad wings, such as those of vultures and eagles. The broad wingtips of these birds are divided by the primary feathers into what are effectively many small wingtips. The small vortices created by the individual feathers create less drag than the one large vortex that would be created without this sub-division. In general large, relatively slow-flying soaring birds will be equipped with such wings, with the relatively large wing chord keeping Reynolds numbers up.

Many birds do not have either of these wing shapes. Guinea fowl, for example, have short, stubby wings with rounded tips. These may not be optimal from an aerodynamic performance point of view, but are nevertheless suited to the needs of the bird. Guinea fowl need to do a lot of flapping to stay in the air and tire quickly, but are agile and able to dart between bushes and trees, enabling them to escape from predators.

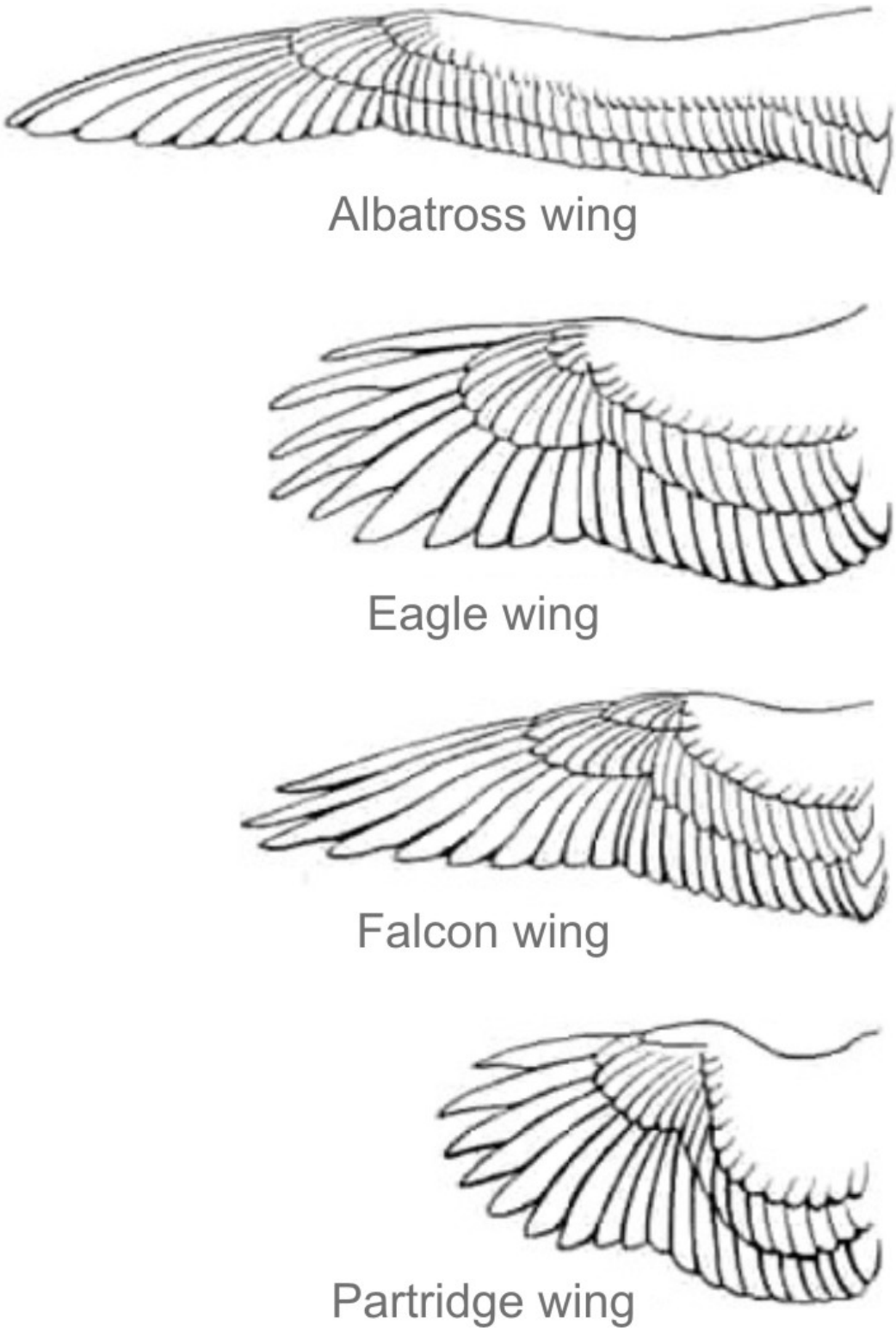

Figure 2.11: The four basic Bird Wing Types (edited from [13])

2.5 Previous Projects by Others

This section will introduce some projects done by other people or organisations. The projects will be grouped according to their solution to the problem of pitch stability. Alongside this the particular aerodynamic solution chosen will be elucidated. Following that, other pertinent elements of these projects will be discussed.

2.5.1 Pitch Stability through the use of a Stable Airfoil

Stability in the pitch axis is also achievable with airfoil sections that are designed to have a positive pitching moment. These airfoils have a camber line that dips below the chord line in the region of the trailing edge ('reflexed' trailing edge). Figure 2.12 shows a typical example, the OSHKCOR4 airfoil [14], computer-generated and used by Bob Hoey in his model of a Turkey Vulture [15]. In a sense these airfoils simply integrate the function of the horizontal stabiliser into the aft section of the airfoil.

Figure 2.12: The OSHKCOR4 Airfoil [15]

This is the simplest solution to the problem of pitch stability and many projects make use of it. Another example project that has used this solution is 'Eddie the Eagle' (see figure 2.13 overleaf). The figure shows top views and a front view of the wings. Also to be seen on the left are the five airfoils used, all showing marked reflex.

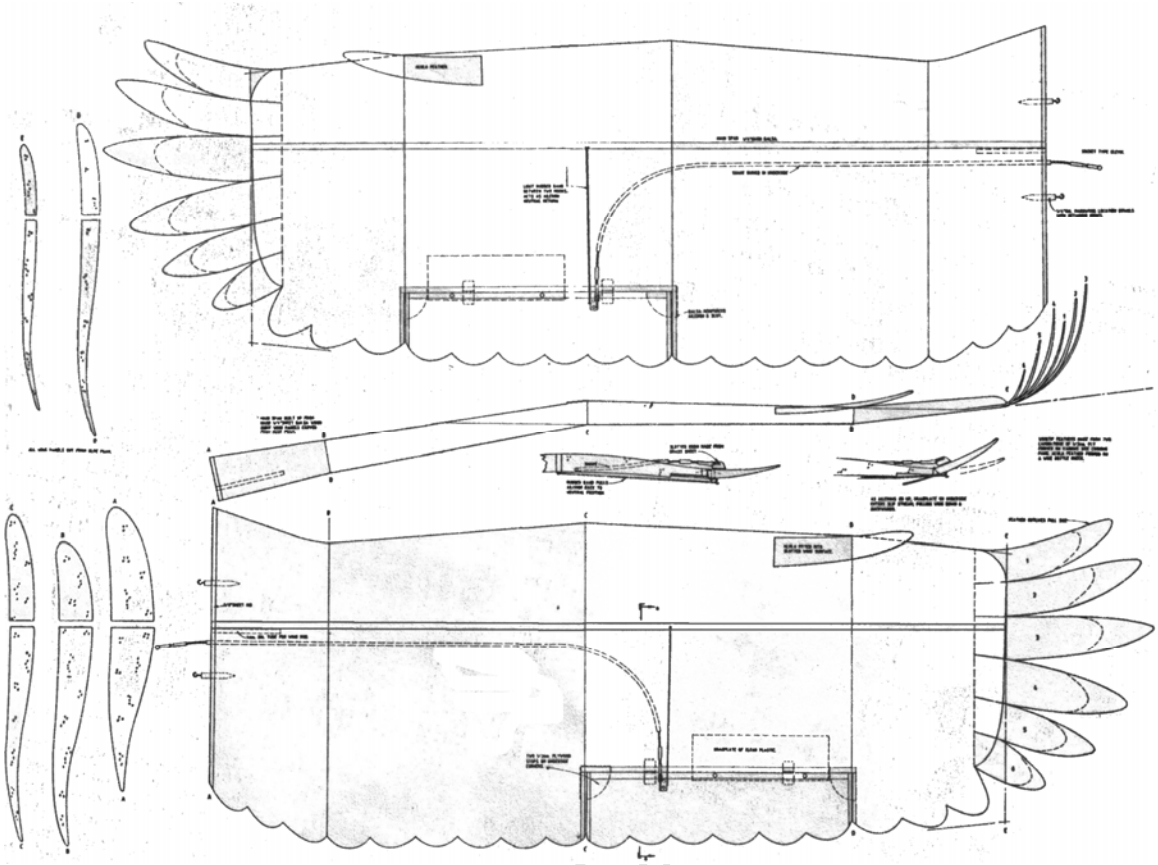

Figure 2.13: Plan View of 'Eddie the Eagle' [16:29]

All other design parameters remaining equal, airfoils with a positive c_{mo} cannot match the performance of conventional airfoils since the reflex trailing edge increases the drag of the airfoil and adversely affects pressure gradients.

As an example, figure 2.14 and figure 2.15 compare the OSHKCOR4 airfoil shown above to what is probably the most well-known airfoil, the Clark Y. The plots were created with 'Profili' [17]. A Reynolds number of 200000 was chosen for the comparison. This corresponds to a 25cm chord wing flying at about 12m/s at sea level.

Figure 2.14 is a graph of lift vs. drag and clearly shows that the Clark Y has a higher maximum c_l than the OSHKCOR4.

The second is a graph of the lift-drag ratio c_l/c_d vs. alpha (the A.O.A) and shows how the Clark Y has a larger usable range of alpha throughout which c_l/c_d exhibits only a gentle slope. The lift-drag ratio of the OSHKCOR4 is lower throughout the entire range except for a very small region (circled in the figure) where it outperforms the Clark Y by a very small amount. However, this is a small region just before the stall and therefore not really usable in practice. Also, the slopes in the usable range of the OSHKCOR4 airfoil are much steeper, showing how the airfoil performs at its optimum in a much narrower range of A.O.A. as compared to the Clark Y.

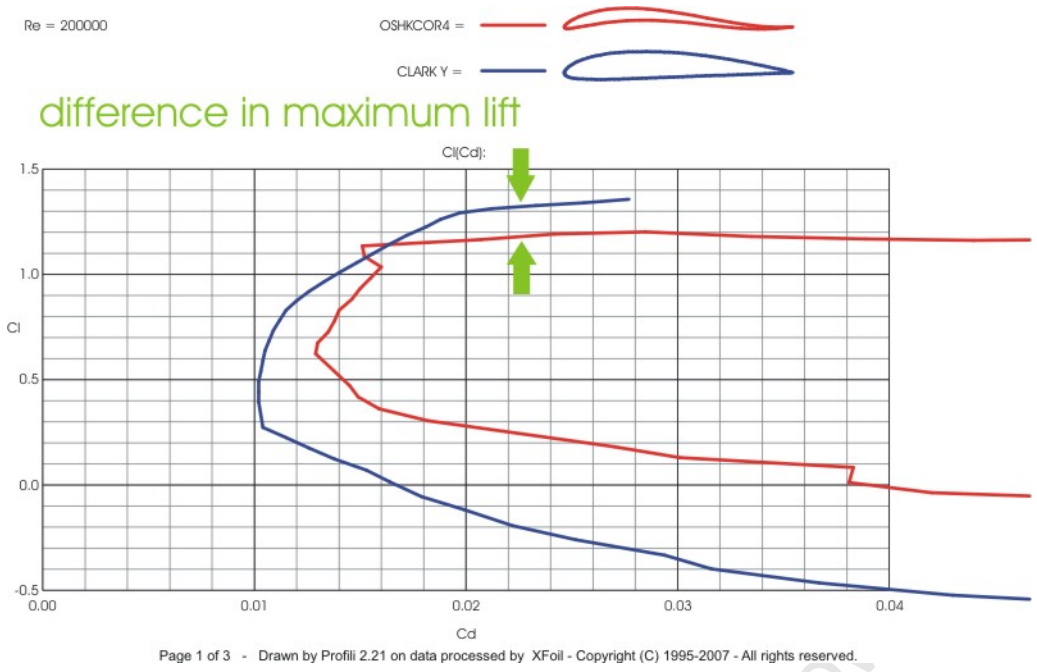

Figure 2.14: c_l vs. c_d Polars for OSHKCOR4 and Clark Y

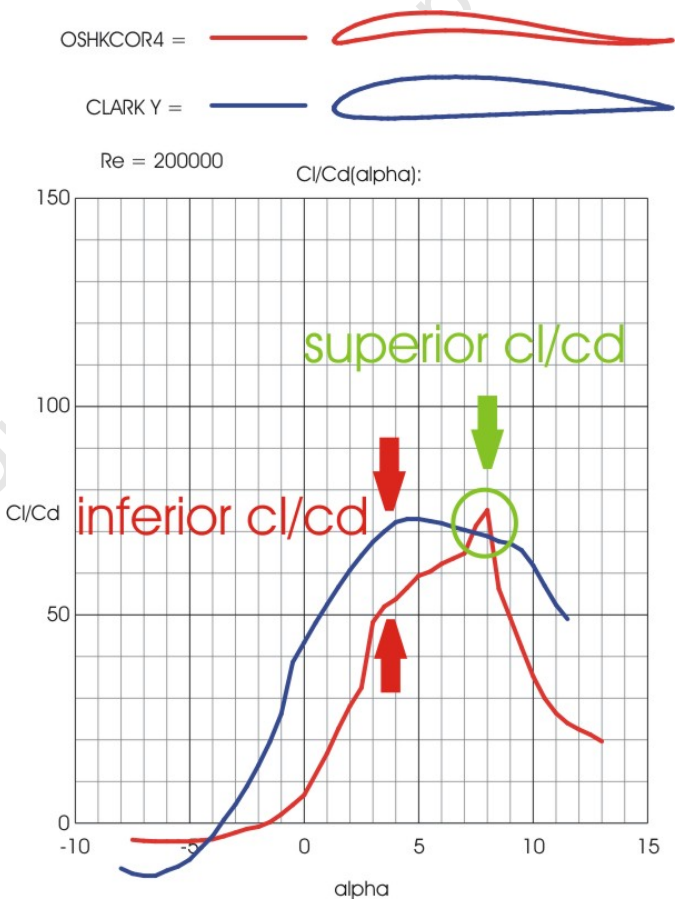

Figure 2.15: c_l / c_d and c_m vs. alpha Polars for OSHLCOR4 and Clark Y

2.5.2 Pitch Stability through the use of Modified Planform Geometry

Some projects retain a sufficiently large margin of pitch stability despite the use of unstable airfoils by modifying the relevant geometry. The 'Emma' seagull design depicted in figure 2.16, for example, lengthens the tail and increases the surface area by a substantial amount (compare with figure 2.17, drawings taken from a real gull by the author). Also, the particularly round contours of this design (see also figure 2.18 overleaf), with the horizontal stabiliser literally being an extension of the body, improve the efficiency of the horizontal stabiliser section.

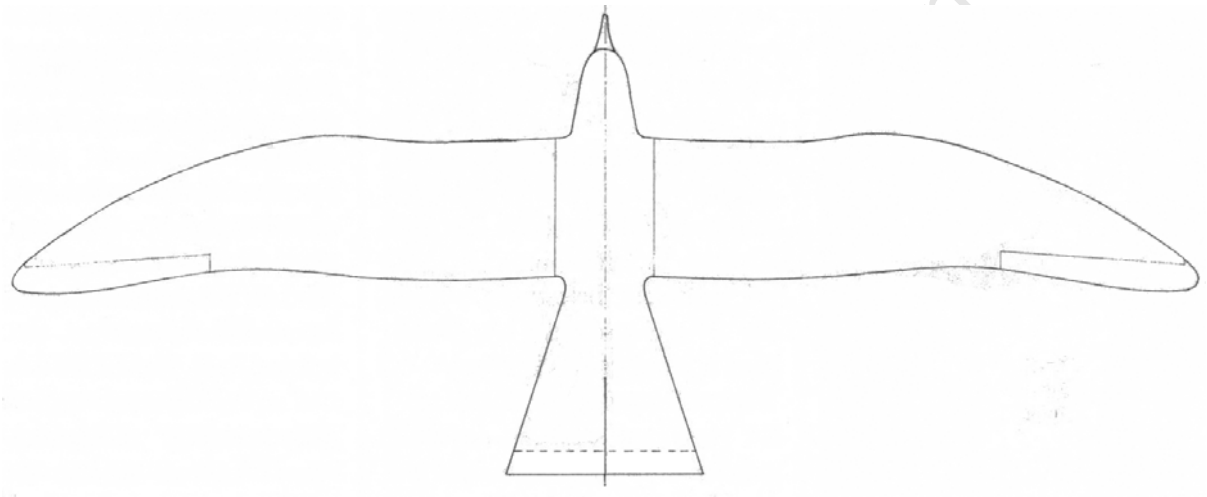

Figure 2.16: Plan View of the Seagull Model 'Emma' [18:21]

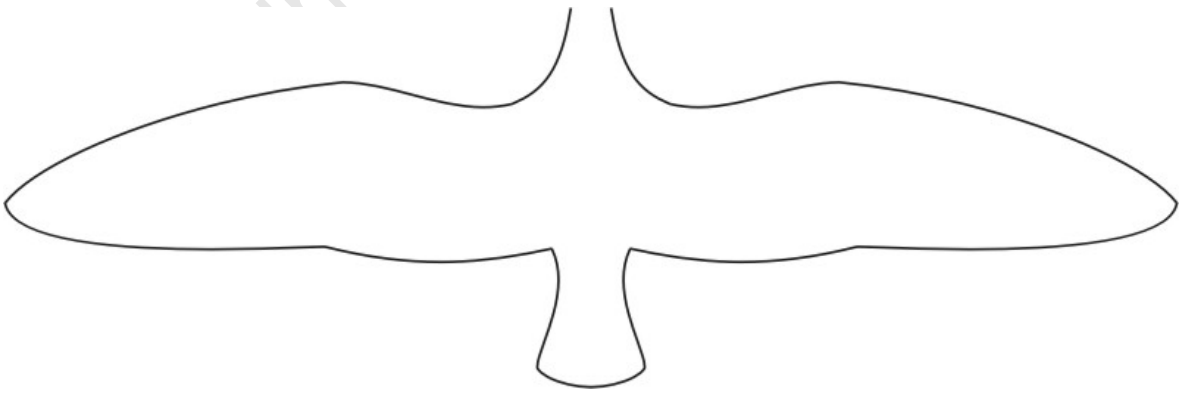

Figure 2.17: Plan View of real Seagull

A peripheral note with regard to this model is that the designer Franz Klement has found a new method of cutting shapes that are curved in all three dimensions out of a block of styrofoam using a regular hot wire styrofoam cutter. The method (which he calls 'Rillentechnik' ('channel technique'), [18]) is labour-intensive but yields very realistically shaped wings with no straight lines. Figure 2.18 shows this well.

Figure 2.18: View of the Seagull Model 'Emma'

2.5.3 Pitch Stability through the use of Modified Wing Geometry

Another way to generate a downward force behind the A.C. of the wing is to use sweepback and 'wash-out' (a decrease in A.O.A. as the wingtip is approximated) as in figure 2.19. In this layout the wingtips perform the function of the horizontal stabiliser while the more inboard section of the wing generates the lifting force. Sweepforward and wash-in has the same effect with regard to pitch stability.

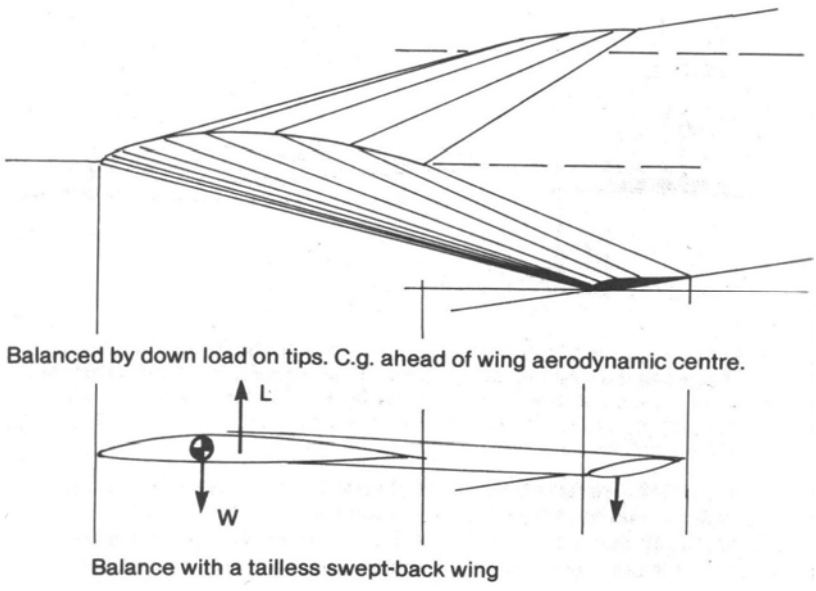

Figure 2.19: Pitch Stability using Sweep and Wash [5:166]

A B.B.C. (British Broadcasting Corporation) production by the name of 'Pterodactyls Alive' features a flying model of a pterodactyl (depicted in figure 2.20). This is not a bird, but the aerodynamic challenges in designing a model are similar.

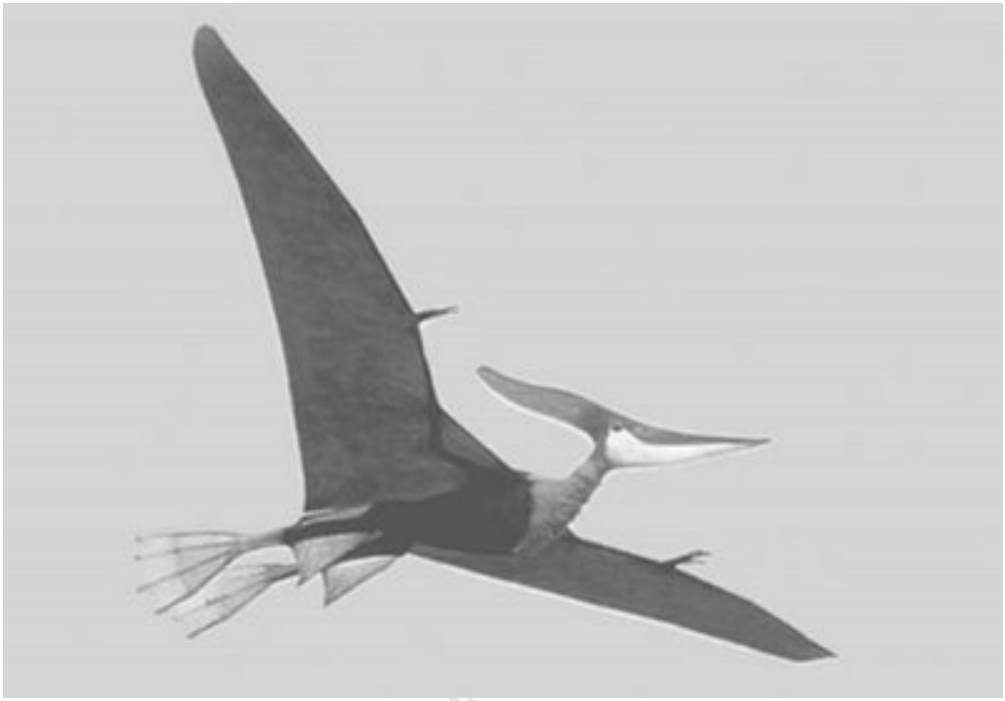

Figure 2.20: Pteranodon from 'Pterodactyls Alive' [19]

This model uses sweepforward and wash-in as well as a reflexed airfoil at the root which changes to an airfoil with a negative c_{mo} at the tip (E184-174). The designer, Stephen Winkworth, makes special mention of the following items:

"… and Professor Eppler, who kindly looked over the design, commented: "It seems that you have not enough sweeps forward for using 174 at the tip." Indeed, when calculated, pitch stability comes out slightly negative… (but by concentrating weight as far as possible below the wing) the slight aerodynamic instability is compensated for by inertial stability, and the result is a model that stays on an even keel for long enough to be quite manageable… [20]"

It may be apparent that the size of the feet and the presence of the vertical surfaces on the upper thighs are not biologically accurate. These items are addressed in chapter 2.5.6.

2.5.4 The Horten Lift Distribution

The ideal lift distribution in terms of induced drag is elliptical (k = 1 in Eqn. 5). If airfoils and aerodynamic wash-out are chosen in a specific way the lift distribution becomes bell-shaped (see figure 2.21), the induced drag at the wingtips becomes negative ('induced thrust') and therefore there is no adverse yaw [21]. This is known as the Horten lift distribution, first implemented by the Horten brothers [22]. No separate horizontal or vertical stabilisers are needed, this is the pure 'flying wing' that is completely controllable with all control surfaces being in the plane of the wing. The increased drag due to the non-elliptical lift distribution ('k' in Eqn. 5 generally becomes about 1.3) may be offset by the lack of form drag from fuselages and stabilising surfaces. The stabilising effect of sweepback on the pitch axis is also made use of in the Horten configuration.

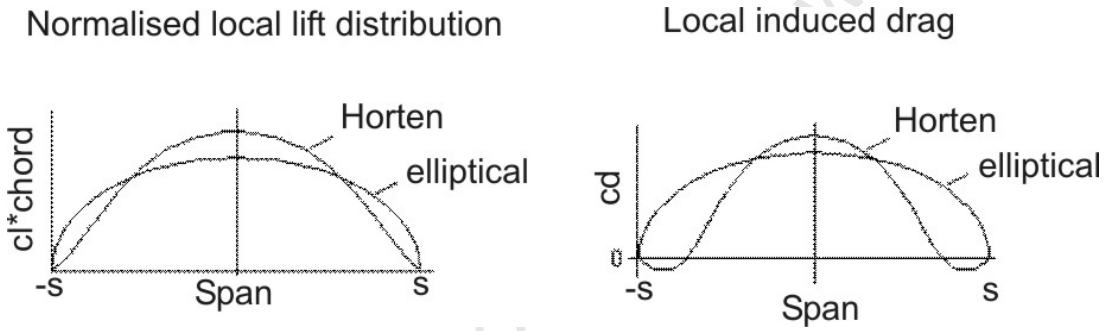

Figure 2.21: The Horten Lift and Drag Distribution (edited from [23])

As an exercise a typical Horten layout was entered into the freeware "Nurflűgel" by Frank Ranis [24]. The result is shown in figure 2.22, with the upper (red) curve showing the Horten lift distribution and the lower (purple) curve showing the induced drag distribution, with the induced drag clearly being negative in the region of the wingtips.

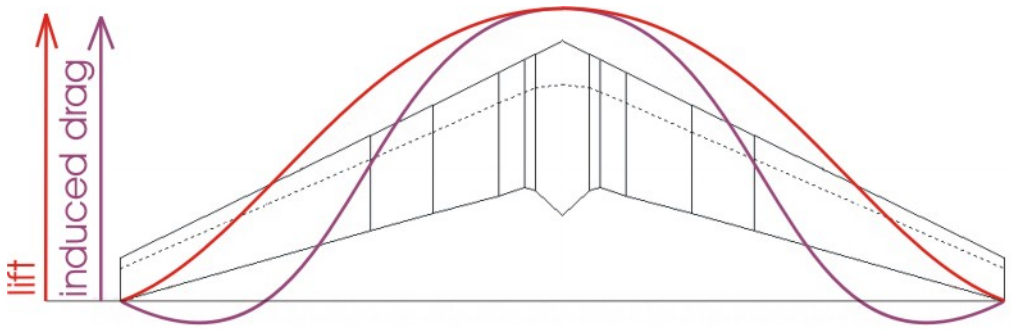

Figure 2.22: Lift and Induced Drag of a typical Horten Layout

The model ‘Milan’ designed by Robert Schweissgut of ‘Ikarus Modellbau’ [25] and shown below in figure 2.23 (built and flown by the author) uses this lift distribution to achieve stability in both the pitch and yaw axes. The tail is only decorative and the model can be flown without.

Figure 2.23: The Model 'Milan'

Due to the choice of airfoils and wash-out angles necessary to achieve the Horten lift distribution for this particular model it can only be flown in a small range of wind speeds. Control is with conventional combined ailerons/elevator (‘elevons’).

2.5.5 Pitch Stability through the Use of Pitch Sensing and Feedback Loops

The half life size model (5.5m wing span) of the pterosaur 'Quetzalcoatlus' by Paul MacCready of the company AeroVironment is worthy of some note [26]. The model is depicted both on the ground and in the air in figure 2.24.

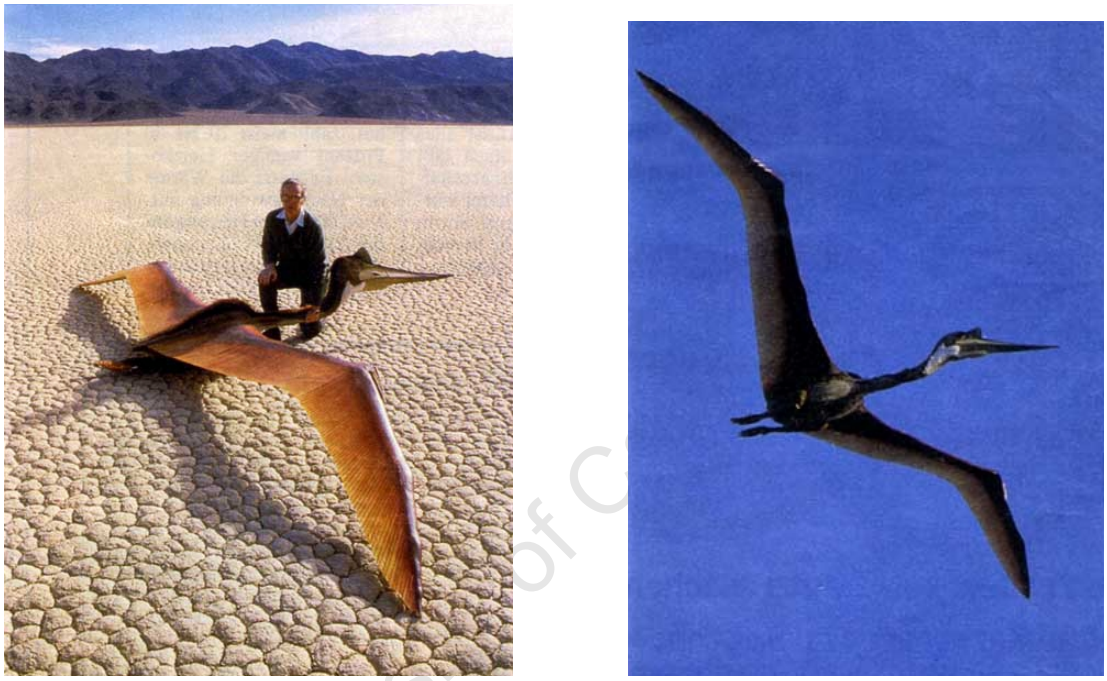

Figure 2.24: The Quetzalcoatlus Model on the Ground and in the Air [27, pg.82]

The model was able to sustain level powered flight by flapping its wings. Pitch stability was achieved by sweeping the wings forwards and backwards and the use of a control incorporating feedback. The control loop, depicted in figure 2.25, was implemented in analogue electronics and made use of an angular rate gyro and a mechanical pitch sensor to correct for the drift of the gyro. The figure gives an idea of the complexity required of the control loop to achieve pitch stability for this model.

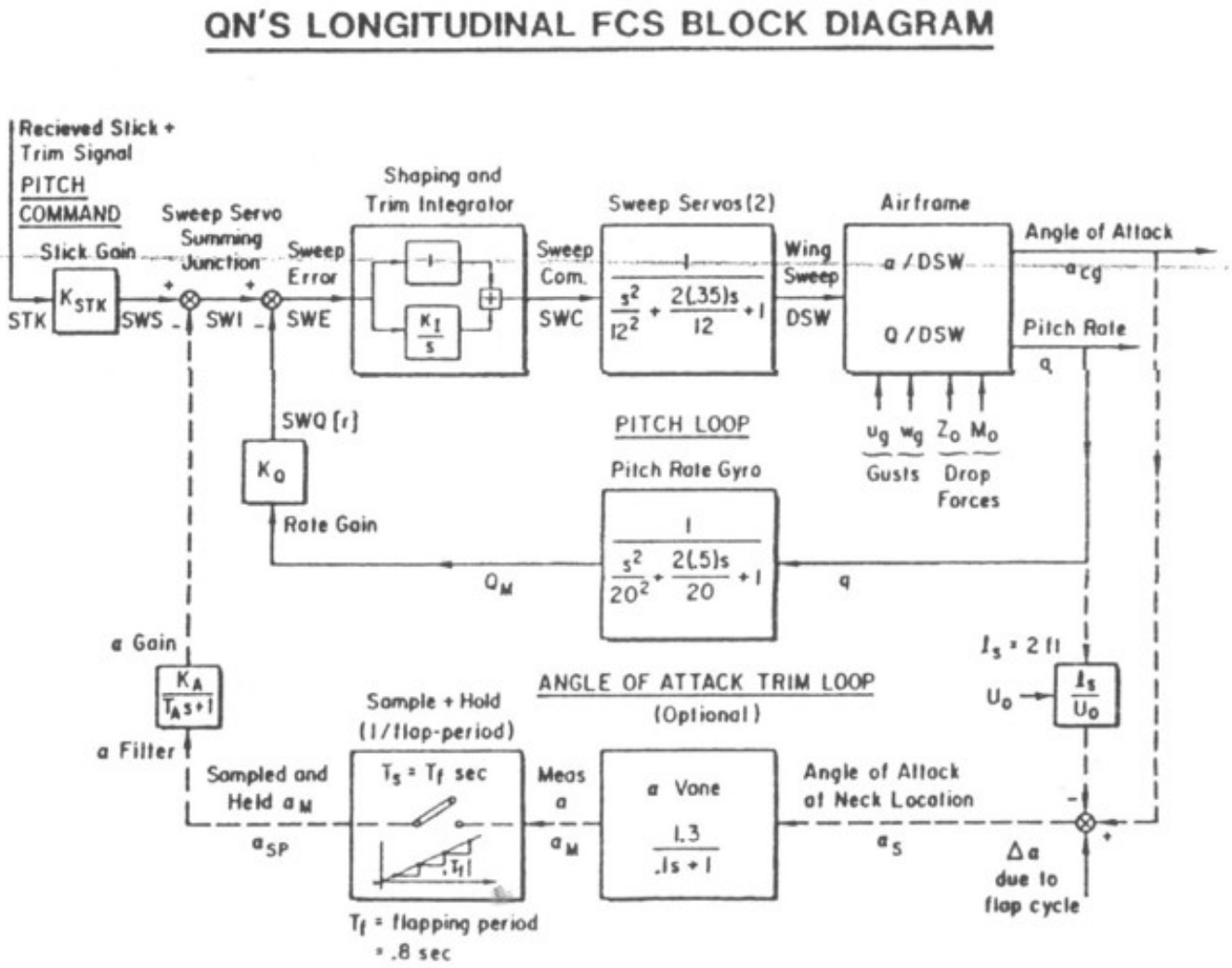

Figure 2.25: Pitch Control Loop for the Quetzalcoatlus Model [28]

A very relevant set of experiments with regard to pitch stability through the use of pitch sensing and feedback loops was conducted by Helmut Lelke [29].

A wing with a conventional unstable airfoil was built and fitted with control surfaces at the trailing edge (see figure 2.26). An A.O.A. sensor and the receiver signal from the radio control unit were the inputs to a control loop that would adjust the control surfaces according to these inputs. Unfortunately there is no real-life picture of the wing in [29]. In figure 2.26 the airflow is meeting the A.O.A. sensor head-on and there is no deflection of the T.E.

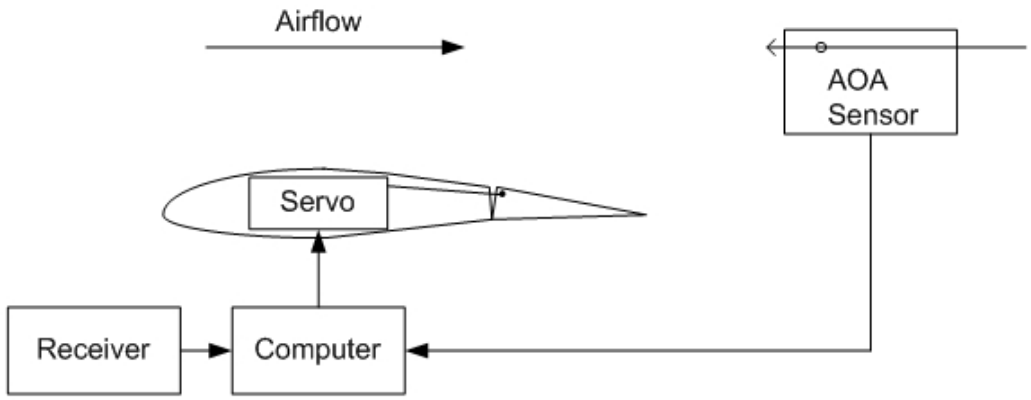

Figure 2.26: Diagrammatic Representation of the Experimental Setup by Helmut Lelke (edited from [30])

If the wing starts to pitch downwards as in figure 2.27, the airflow meets the A.O.A. sensor from the top and the T.E. is deflected upwards, thereby increasing the c_{mo} and creating an upward pitching force to level the wing out.

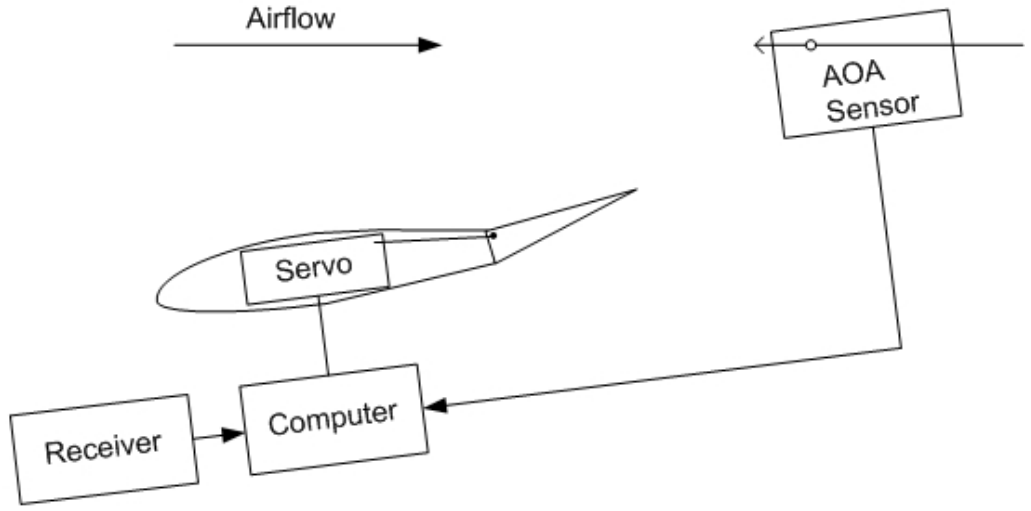

Figure 2.27: Control Surface Reaction to Wing pitching down (edited from [30])

When the wing starts to pitch up as in figure 2.28, the airflow meets the A.O.A. sensor from the bottom and the T.E. is deflected downwards, thereby decreasing the c_{mo} and creating an downward pitching force.

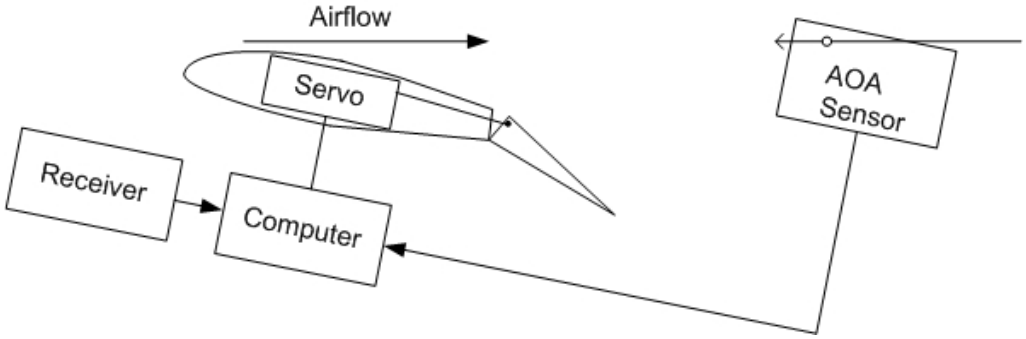

Figure 2.28: Control Surface Reaction to wing pitching up (edited from [30])

As the experiment progressed the neutral position of the T.E. was brought down and the C.G. moved back to compensate. It was found that the wing was stable despite the negative c_{mo} as long as the following conditions were met:

- The gain of the control loop needed to be sufficiently high, as shown in the graph in figure 2.29.

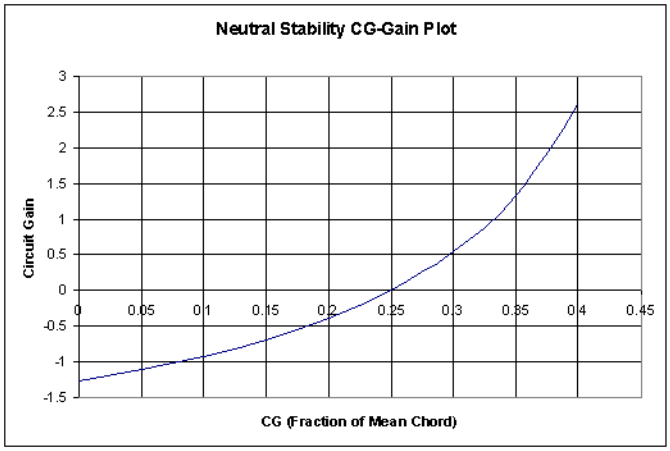

Figure 2.29: Graph of required Circuit Gain for a particular Position of the C.G. [30]

- The speed with which the control surfaces responded needed to be sufficiently fast, where the speed necessary is dependent on how far back the C.G. is to be taken.

This experiment as well as the Quetzalcoatlus project shows that it is within practicably achievable boundaries to stabilise a flying object that is unstable around the pitch axis through the use of feedback.

2.5.6 Solutions to the Problem of Yaw Stability

The various projects listed all also have to solve the problem of yaw stability to some degree or other and various solutions have been applied. These will now be discussed.

'Eddie' uses flat vertical surfaces to model the legs and talons of the eagle, as may be seen in figure 2.30. (The figure is scanned from an old photocopy and thus not very clear.)

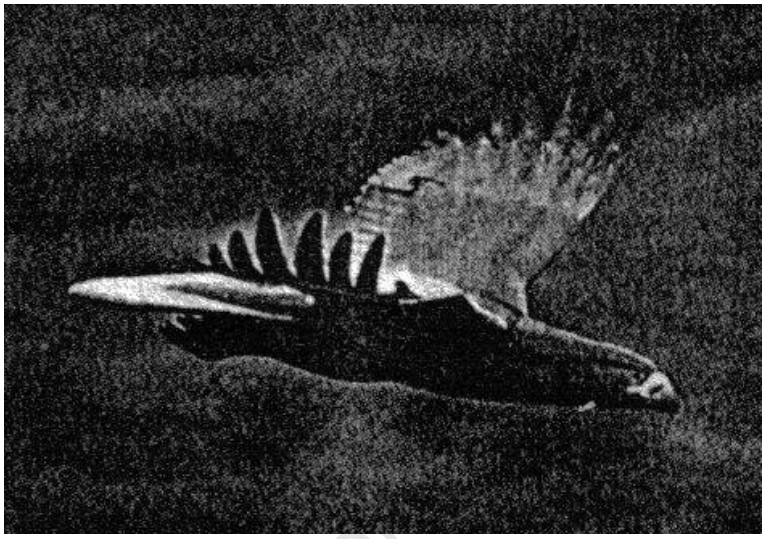

Figure 2.30: Side View of 'Eddie the Eagle' [16:26]

Also, the bent up primaries yield some vertical surface area and thereby assist in stability in the yaw axis (this is to be distinguished from the effect discussed in [10]). The lever arm with regard to both of these items is rather short but seems to make the model sufficiently stable in straight flight. The problem of adverse yaw is addressed by the use of 'split ailerons', i.e. only the aileron of the down-going wing is given a negative deflection and the other aileron does not move, and the use of drag plates ('frise' ailerons) that increase drag on the aileron that is negatively deflected. These can be seen in the planform view in figure 2.13. The use of the frise ailerons only (no rudder) does not allow for separate control of yaw and roll.

The 'Emma' seagull model simply uses a transparent plexiglas vertical stabiliser mounted on the tail for yaw control. Despite the transparency this does reduce the realism of the model.

The pteranodon model has been given disproportionately large feet and some additional vertical area behind the A.C. through the addition of fins to the upper thighs (see figure 2.20). This was necessary to counteract the destabilising effect to yaw of the sweepforward and the large beak and crest at the top of the head.

The 'Milan' model, as previously described, makes use of the Horten lift distribution and therefore has no need for a vertical stabiliser.

The quetzalcoatlus model makes use of a yaw rate gyro and feedback loop (see figure 2.31) as for the pitch control. Again, the figure gives an indication of the complexity of the yaw control task for this model, with multiple inputs (such as 'Turn Rate Command', 'Sensed Sideslip' and 'Rate Gyro and Filter') being processed and generating multiple outputs (such as 'Roll', 'Heading' and 'Path').

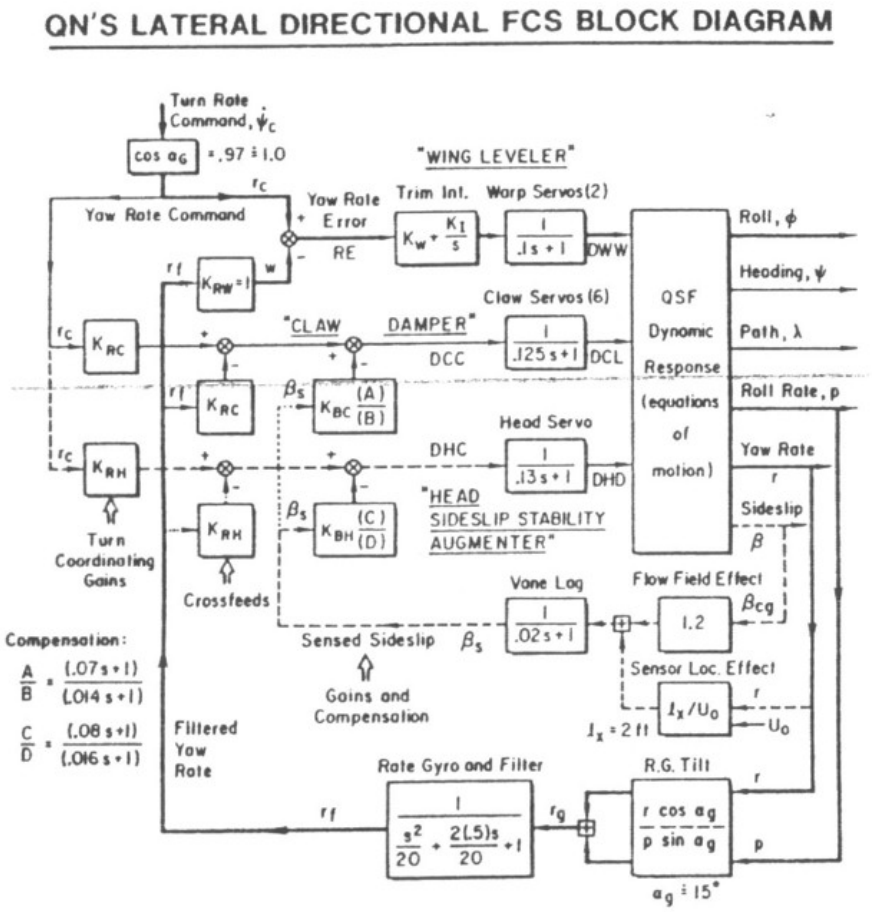

Figure 2.31: Yaw Control Loop for the Quetzalcoatlus Model [28]

Control is successful but the controlling motion of the head is clearly visible in flight. [31]

2.6 The Dissection at the South African Museum (Iziko)

The aim of the dissection was to gain an understanding of the relevant body mechanics as well to have prototypes for various parts of the bird. The specimen offered by Iziko was a Cape Vulture, shown in flight in figure 2.32. The cause of death was electrocution from power lines, which damaged the inner parts of the right wing, hence some results pertaining to this part of the wing (such as weights of feathers) are missing. The results are discussed below.

Figure 2.32: Cape Vulture in Flight [32] and [33]

2.6.1 The Element of Weight

The entire bird weighed 9950 grams. The wings weighed 850 grams each, thus about 83% of the bird's weight is in the body. This has the following benefits:

- Pitch stability is positively affected by having the bulk of the mass hanging under the level of the wings. Note also how high the shoulders are set compared with just about any other type of bird, increasing the vertical distance between the C.G. and the A.C. (figure 2.33).

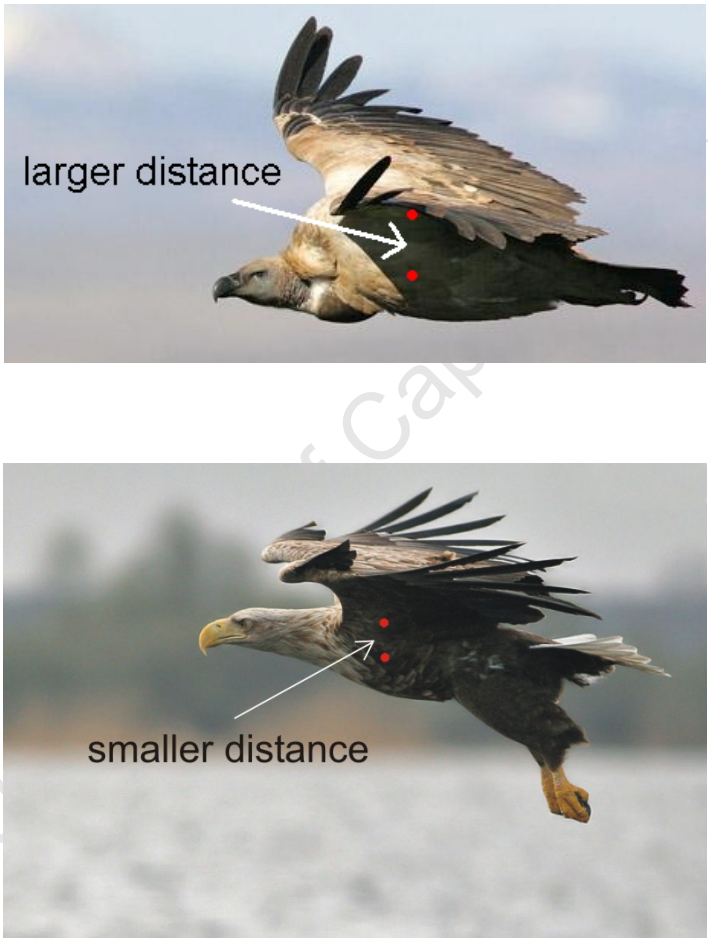

Figure 2.33: Qualitative Comparison of vertical Distance between A.C. and C.G. in Vultures and Eagles (edited from [34] and [35])

- The more the weight is kept close to the C.G. the smaller the forces that are required to produce movements in the roll, pitch and yaw axes.

The weights of the feathers were also documented. The results are shown in figure 2.34. Left and right sides are found to match up extraordinarily well, with the average difference in the weight of corresponding feathers on left and right sides (using feathers 1 through 14) being 0.8%. Numbering starts at the tip and the count ascends as the body is approximated.

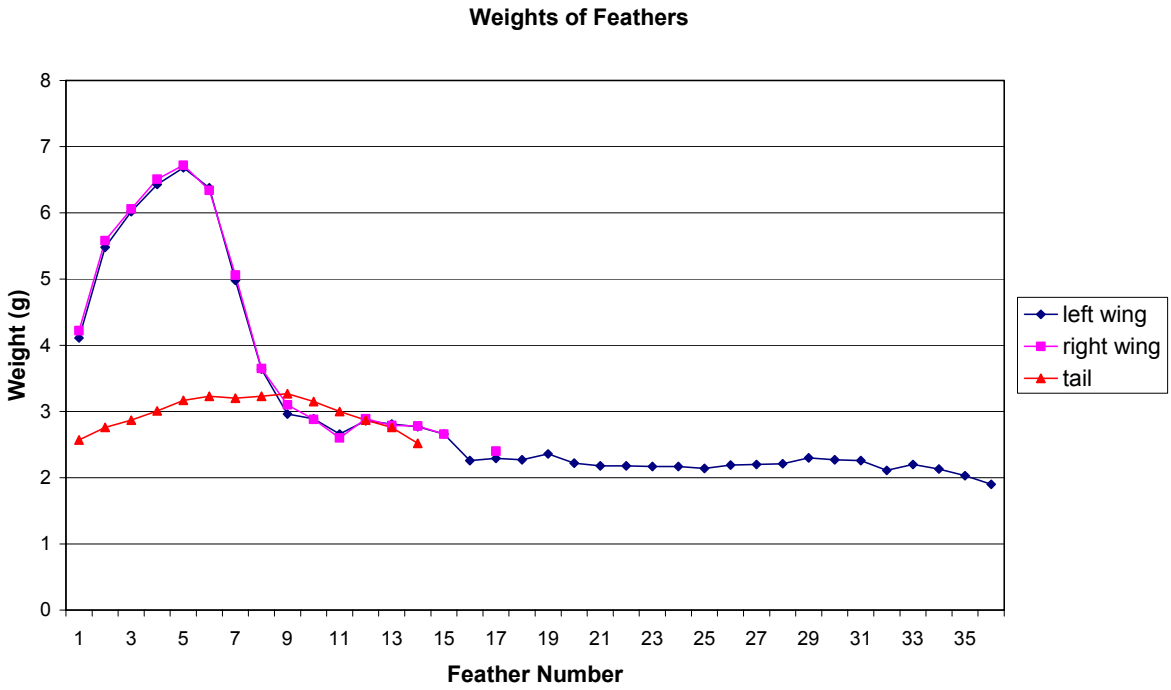

Figure 2.34: Figure showing the Weights of different Feathers

Of the 850 grams for the wing, 350 grams were accounted for by the complete set of feathers and a small amount of connective tissue. The bones made up 190 grams of the wieght. This means that about 59% of the weight of the wing is very close to the L.E. of the wing, especially from the wrist in the outboard direction where the L.E. is directly shaped by the bone and not the propatagium as it is between the shoulder and the wrist. This affects the mechanical stresses on the wing during flight (resistance to wing flutter is enhanced, [36]) and would thus need to be observed in construction.

The above reference contains an interesting anecdote involving the McDonnell Aircraft Company and a captured Russian MiG-15. It ends with “While it is deliberate heresy to consider ballast weight in an airplane, this is one case of one pound ballast replacing over 12 lbs. of structure.” [36:149].

2.6.2 The Shapes of the Feathers

The shapes of the feathers, in particular the primaries, were of some interest. The primaries are of particular interest since, when the wing is stretched, a significant part of each one is a wing in its own right, not touching another feather but moving freely through the airflow and significantly affecting the aerodynamics of the wingtip. A rig to measure the local angles of attack along the feather was constructed (see figure 2.35).

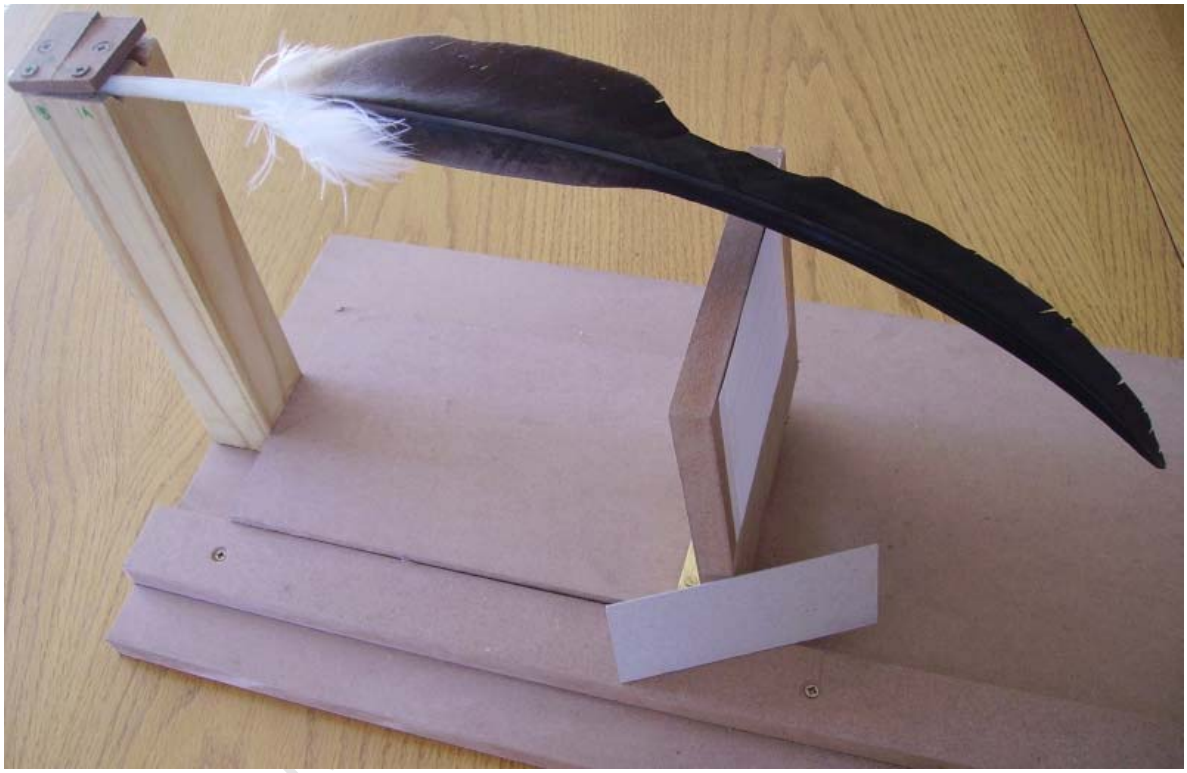

Figure 2.35: The Feather Measurement Rig

The feather to be measured was marked at regular intervals and clamped into place. The hinged wooden unit could be slid back and forth under the feather, with the hinge permitting the wooden board with a piece of paper stuck to it to be oriented at right angles to the curve of the rachis. A small piece of cardboard with straight edges was then placed partially onto the wooden board and also aligned with the L.E. and T.E. of the feather and the line of the bottom edge marked on the paper. Once this was done the lines on the piece of paper (see figure 2.36 for an example) were measured and entered into a spreadsheet that calculated the associated angles.

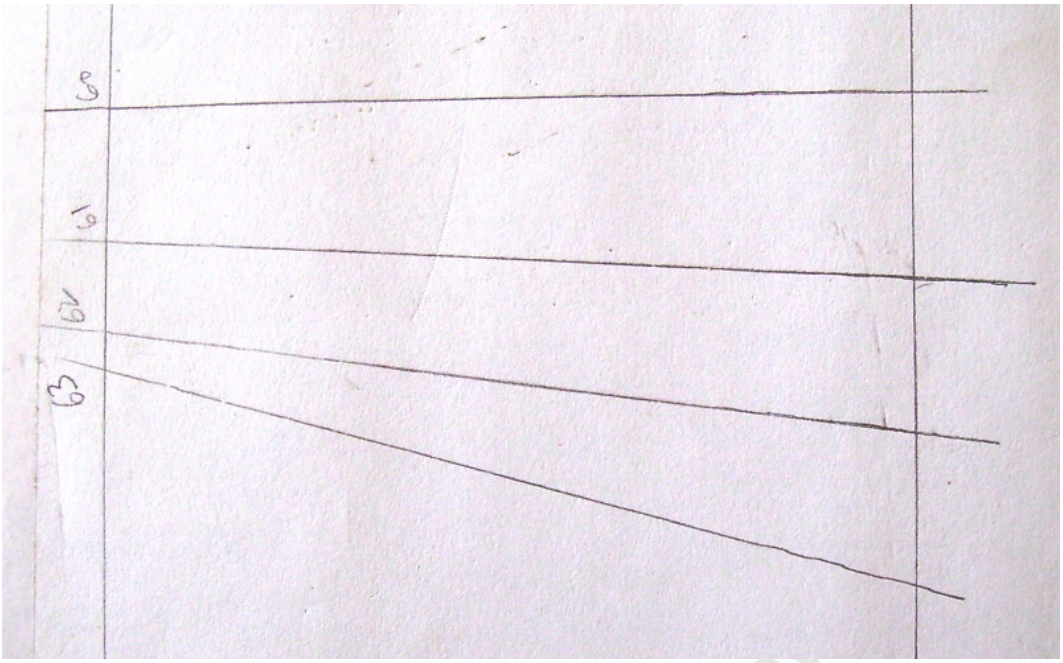

Figure 2.36: Example of Measurements taken

Another parameter that was measured was the camber distribution along the span. Since the thickness of the vane is negligible, the camber was viewed as being the vertical distance between the line joining the leading and trailing edges and the highest point of the rachis in a cross-sectional view of the feather. The angle at that part of the feather where the emargination ends was defined as zero degrees and the distance at that point as zero, since that is where the feathers stop overlapping and each becomes its own 'wing' when the wings are stretched. Figure 2.37 and figure 2.38 show the results for these two experiments, along with linear or polynomial approximations. Note that the last point displayed on the graph does not represent the tip since the tip, being a point, is unsuitable for an angular measurement.

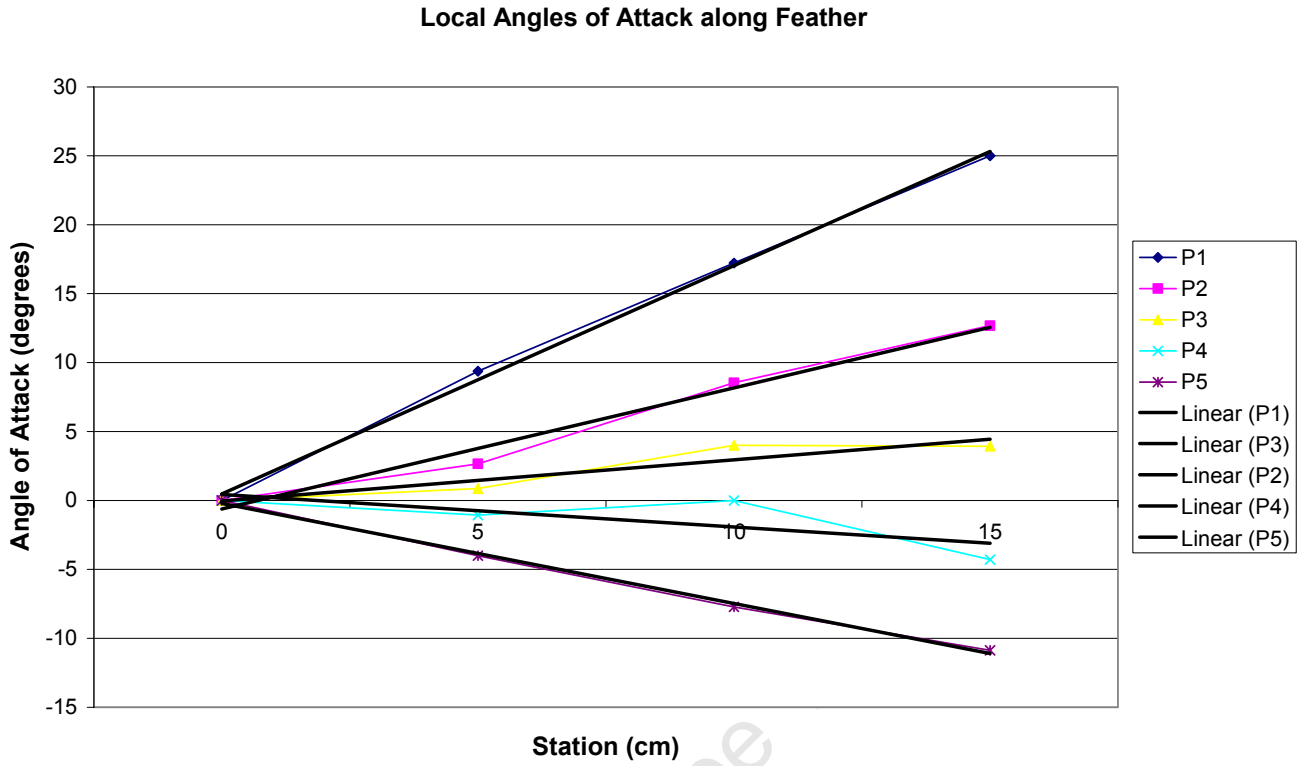

Figure 2.37: Graph showing the local Angles of Attack along the Feather

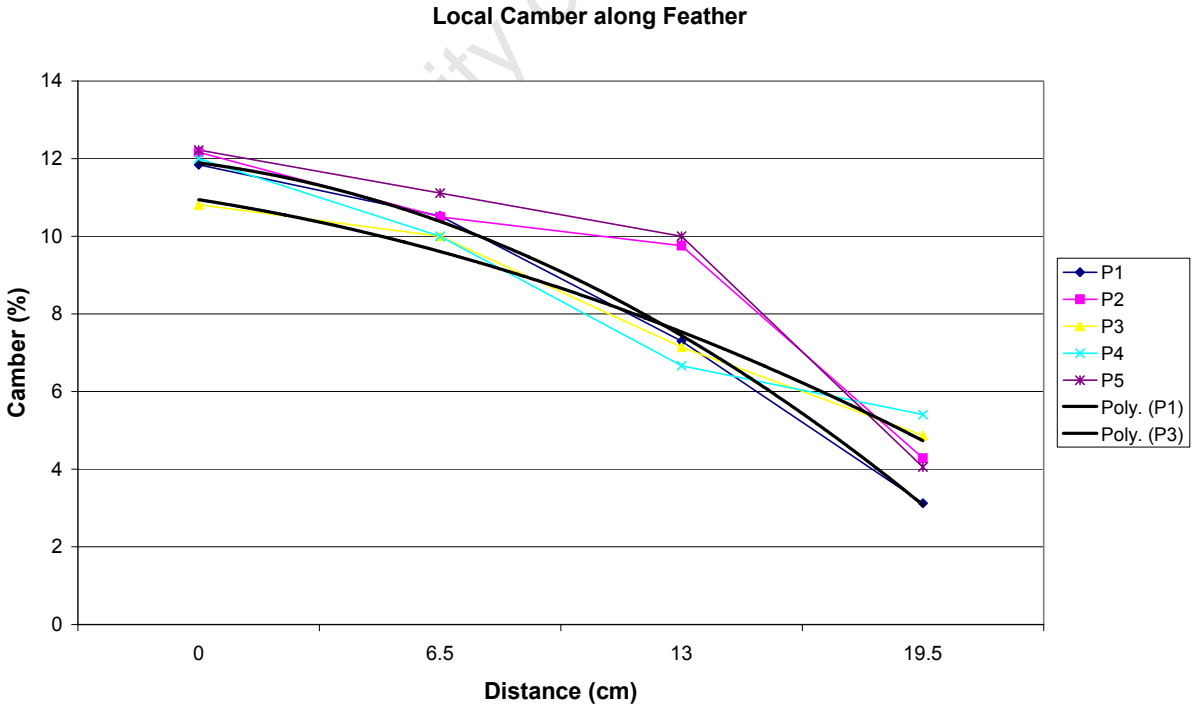

Figure 2.38: Graph showing the Variation of Camber along the Feather

The results show that the A.O.A. changes linearly along the span of the feather (after the emarginations) and that the camber changes non-linearly, decreasing slowly at first and more rapidly later. Also, the maximum A.O.A. decreases fairly linearly from feather to feather, with the decrease from P1 to P2 being a little larger than the rest. These parameters are obvious candidates for inclusion into any model of the feather.

A very intriguing item is the fact that the first three feathers show wash-in, with P1 peaking at around 30°. Any model aircraft wing designed along these lines would not be controllable. In general, a model glider wing is designed with geometric wash-out or, better yet to ensure that all points along the span reach zero lift at the same A.O.A, a combination of geometric and aerodynamic wash-out. Geometric wash-out refers to a decrease in the angle of attack towards the tip, whereas aerodynamic wash-out is brought about by a change in the airfoil towards the tip. Wash-out ensures that, all other things being equal, the root of the wing stalls first and the aircraft remains controllable. A tip stall, due to the sudden increase in drag at one tip only, tends to yank the glider around the yaw axis and control is compromised.

Each of the feathers is of course only a part of the entire wingtip and the aerodynamics of this part of the wing is very complex. The scope of this project is insufficient to investigate in detail how the wash-in of the primaries affects airflow around the wingtip. One suggestion that can be made is the idea that a local lift force is generated in front of the A.C., thereby contributing a positive pitching moment to counteract the negative pitching moment of the entire wing in the same manner that the downward force of the horizontal stabiliser behind the A.C. does in a normal airplane configuration (see figure 2.9). The perspective in figure 2.39 shows how P1 is twisted during flight (wash-in) by the way in which the L.E. and T.E. of the feather cross.

Figure 2.39: Wingtip showing twisted Primary in Flight (zoomed from [37])

2.6.3 Chapter Conclusion

It is hoped that the reader has been able to gain some insight into the difficulties surrounding the challenge of designing a flying bird robot that looks like a bird and is both stable in flight and controllable by means based on the movements of the bird in flight rather than separate hinged control surfaces. The investigation into the feathers yielded relevant information that any design would need to take into account.

Having gained this knowledge it was time to isolate a particular facet of the design and conduct a practical investigation into it.

3 The Proposed Experiment

3.1 Chapter Introduction

From all of the above it became clear that a full reconstruction involving all of the aspects discussed was not feasible in the context of this project. It was decided that an investigation into the effects of the motion of the tail would be of interest. If the forces generated by different positions of the tail were to be known it would be possible to include these in a control scheme for a bird robot. Since the tail can move both up and down as well as rotate around the axis of the spinal column, it should be possible to vary the forces around the pitch, roll and yaw axes by moving the tail. This is particularly pertinent since it has been shown that the functions of the tail are different when comparing birds and conventional airplanes.

The experiment was to be conducted in the following manner:

A life-size model of the body was to be built. The tail was to be made movable and able to rotate around both the pitch and roll axes. The model was to be put in a wind tunnel and the forces generated by different positions of the tail noted. From this it should be possible to derive a function that predicts the forces generated for a particular position of the tail, which has become the aim of this project.

3.2 The Experimental Setup and Related Considerations

For the preliminary description of the experimental set-up figures 3.1, 3.2 and 3.3 may be referred to. Figure 3.1 shows the real-life model whereas figures 3.2 and 3.3 show SolidWorks images. SolidWorks is the software that was used to design the mechanical implementation of the model. Note that figure 3.2 does not show the polystyrene sides that give the body its shape since these were not modelled. More detailed figures of individual parts follow. The all-up weight of the model was 1.650 kg. However, since none of the measurements involved dynamic effects the weight is not relevant to these. Consideration of the inertia of the model only becomes relevant when viewing the video clip referred to at a later point.

Figure 3.1: Image showing complete Model

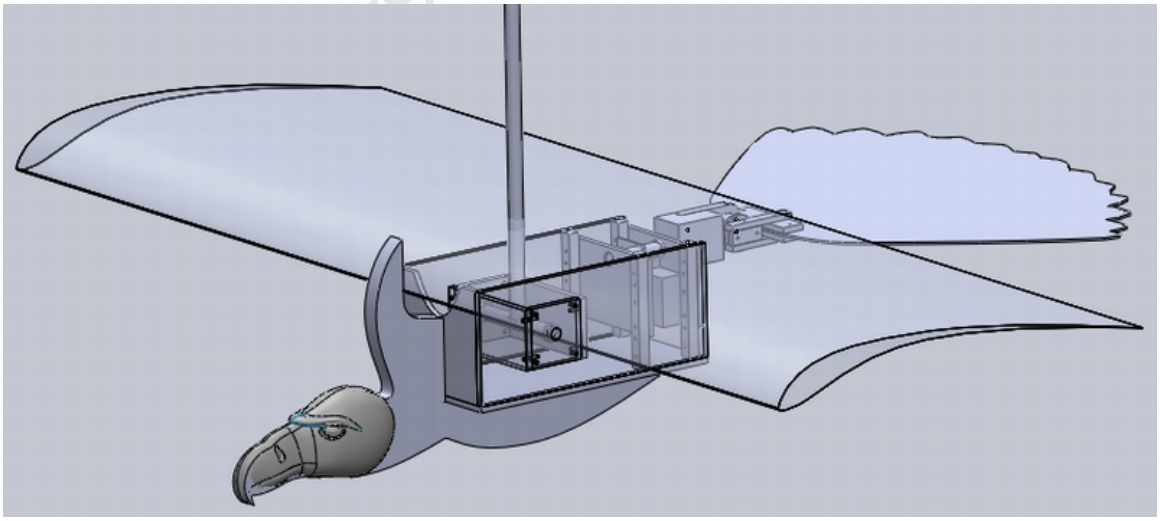

Figure 3.2: Complete View of the Model as created in SolidWorks

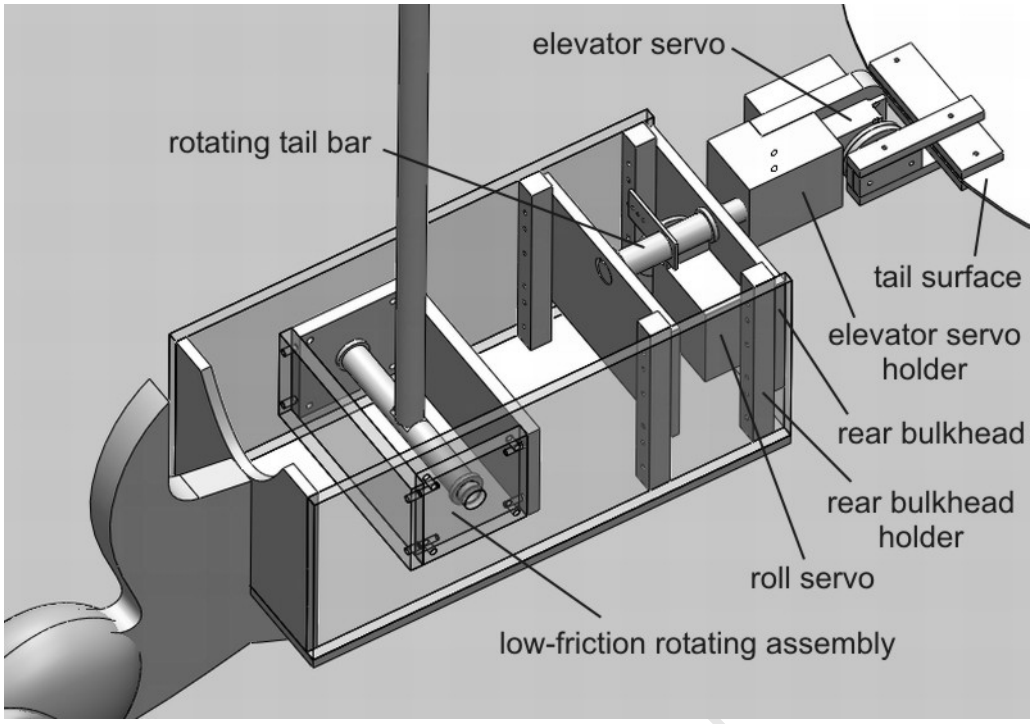

Figure 3.3: Closer View of Model detailing Parts

The main structure of the body was made up from plywood, polystyrene and styrofoam. The tail unit was connected to the front part of the body via the rotating tail bar. In this way the tail could be rotated by moving the roll servo. The elevator servo moved the tail up and down.

3.3 Parts of the Experimental Setup in Greater Detail

The following paragraphs detail relevant aspects of and considerations with regard to the individual parts of the experimental setup.

3.3.1 The Body Shell

The body shell was constructed from 5mm plywood parts that were designed in SolidWorks and cut by a laser cutting machine. Expanded polystyrene, cut and sanded, was used to give the body its final shape. A small section at the top of the body between the shoulders was left open to allow the suspending rod some degree of movement.

The polystyrene and foam was left with its natural surface roughness after sanding to simulate the surface roughness resulting from the feathers of the vulture.

3.3.2 The Rotating Assembly

The rotating assembly (see figure 3.4) is what provided the entire body structure with its one degree of freedom in the wind tunnel.

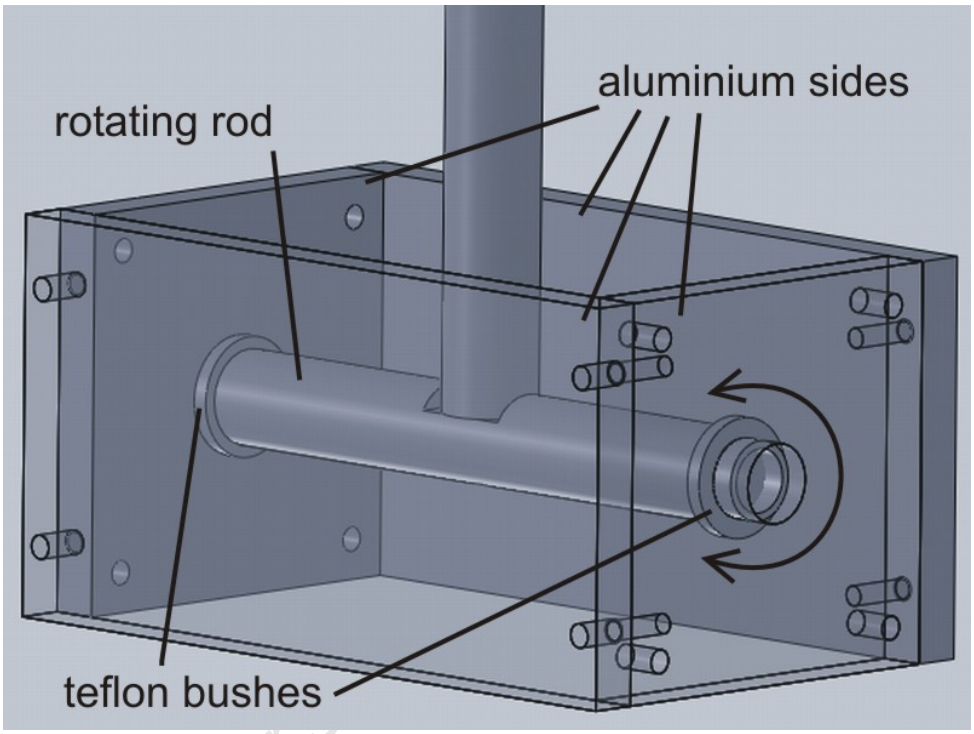

Figure 3.4: The Rotating Assembly

The 'box' (open at the top and bottom) consists of aluminium sides, screwed together. Bushes in two of the faces allow a central rod to rotate freely as indicated by the arrow in the figure, and another rod connected to the middle of the first allows the entire assembly to be connected to the top of the wind tunnel.

When in the configuration as shown in figure 3.4 the degree of freedom offered is around the pitch axis or the roll axis, depending on the orientation with which the assembly is mounted within the model.

For measurements with regard to the yaw axis there is a similar re-orientation of the rotating assembly, but in addition the vertical bar needs to be removed and re-attached along the axis of the bar that rotates in the bushes, as shown in figure 3.5.

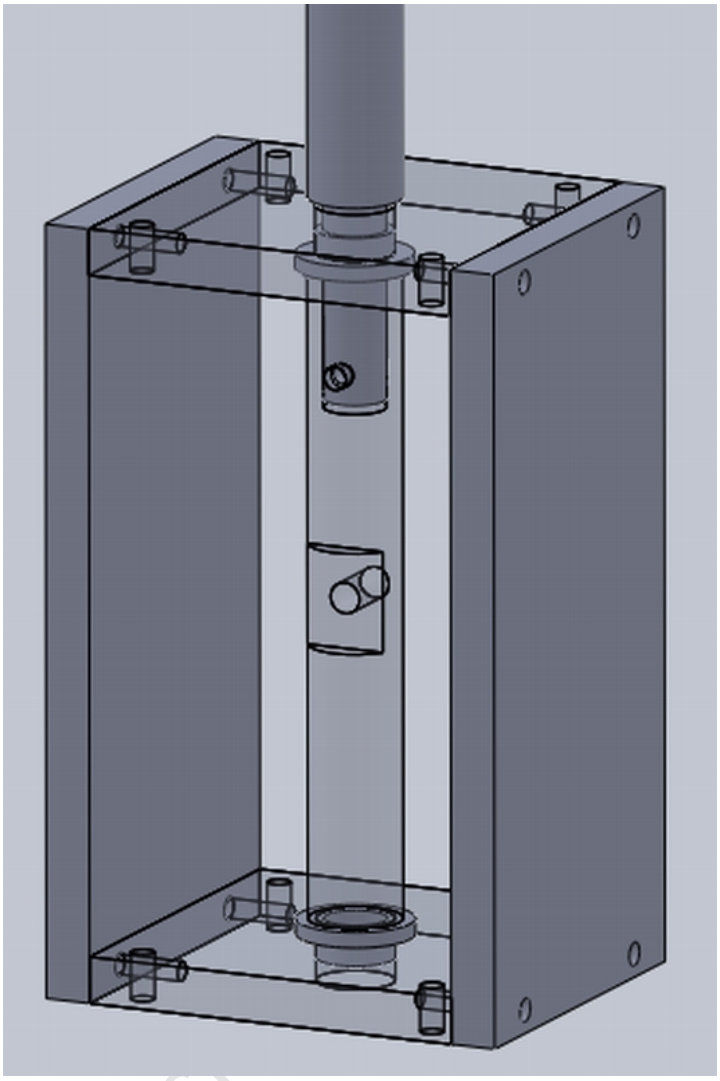

Figure 3.5: Rotating Assembly in Vertical Orientation

3.3.3 The Bulkheads and Tail Bar

The middle and rear bulkheads were made from 5mm plywood. They served as holders for the rotating tail bar. Again, teflon bushes between the bulkheads and the tail bar reduced friction between these two items.

3.3.4 The Elevator Servo Holder

The elevator servo holder is simply the mechanical connection between the tail bar and the elevator servo. It was machined from aluminium.

3.3.5 The Elevator Servo

The elevator servo sits in the elevator servo holder and makes it possible to move the tail up and down. To eliminate linkage slop the tail was mounted directly on the servo output disk. Thus only backlash from the servo gearing is present.

3.3.6 The Tail

The tail was made from 3mm plywood and mounted directly on the elevator servo with an arrangement made from 5mm plywood.

3.3.7 The Rod Holder

The rod holder attaches to the top of the wind tunnel and, together with the connecting rod, connects the movable model to a stationary reference point.

3.3.8 The Electronics

The servos were controlled by the use of a laptop, a power supply, a cable carrying power and control signals and a servo control board. Matlab code running on the laptop was used to send signals to the servo control board through the serial port. The servos, connected to the servo control board, responded according to the values entered on the laptop.

3.3.9 Measurement Points

Figures 3.6 and 3.7 show the loops into which the spring balances were hooked during the experiments. The black markings in the front section of the airfoil in figure 3.7 were reference points during construction and have no meaning. The distance between the point of measurement of forces around the pitch axis and the point around which the model rotated during the pitch experiments was 0.29m. The equivalent distance for the yaw and roll experiments was 0.5m. These values are important for converting the measured forces into torques.

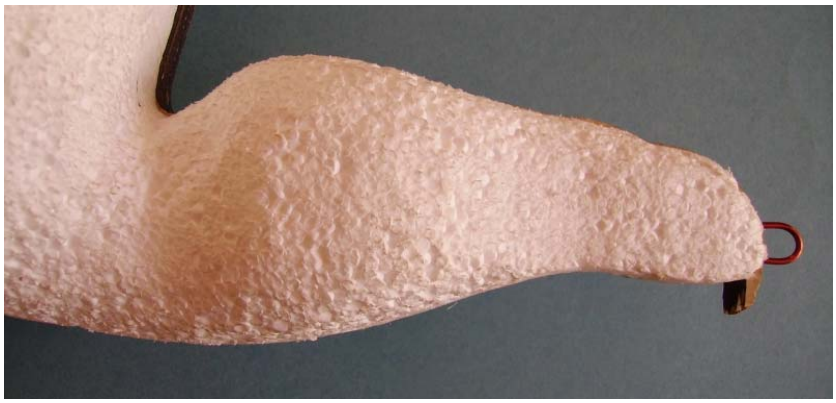

Figure 3.6: Figure showing the Measurement Point for the Experiments involving the Pitch Axis

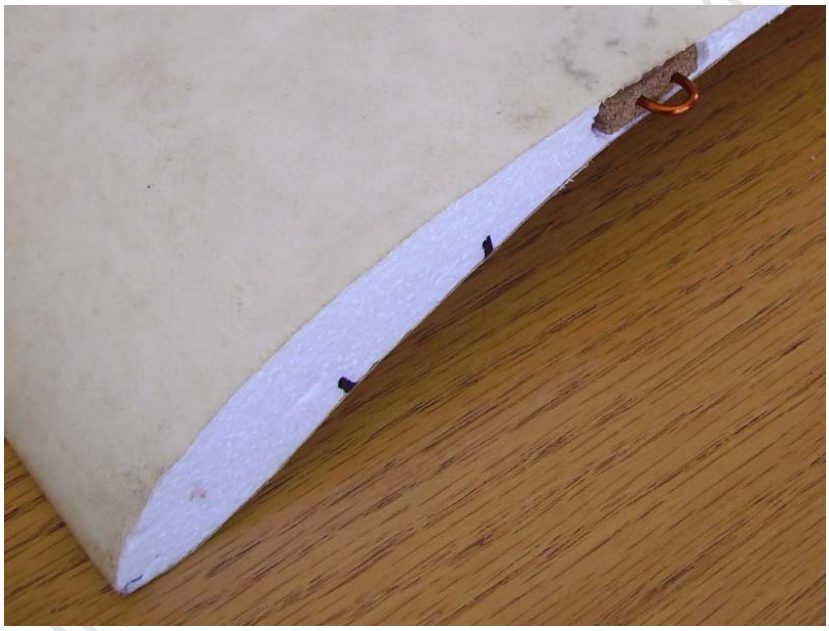

Figure 3.7: Figure showing the Measurement Point for the Experiments involving the Roll and Yaw Axes

Figures 3.8 and 3.9 overleaf show photos of the inside of the finished model. Figure 3.8 shows the rotating assembly in the position that it would be in for measurements in the yaw axis. The wing mount platform allows the wing to be bolted to the body.

Figure 3.9 focuses on the back of the model and shows a close-up view of the elevator servo and holder. Also to be seen are the rotating tail bar and one of the teflon bushes that ensure a smooth low-friction movement of the tail bar.

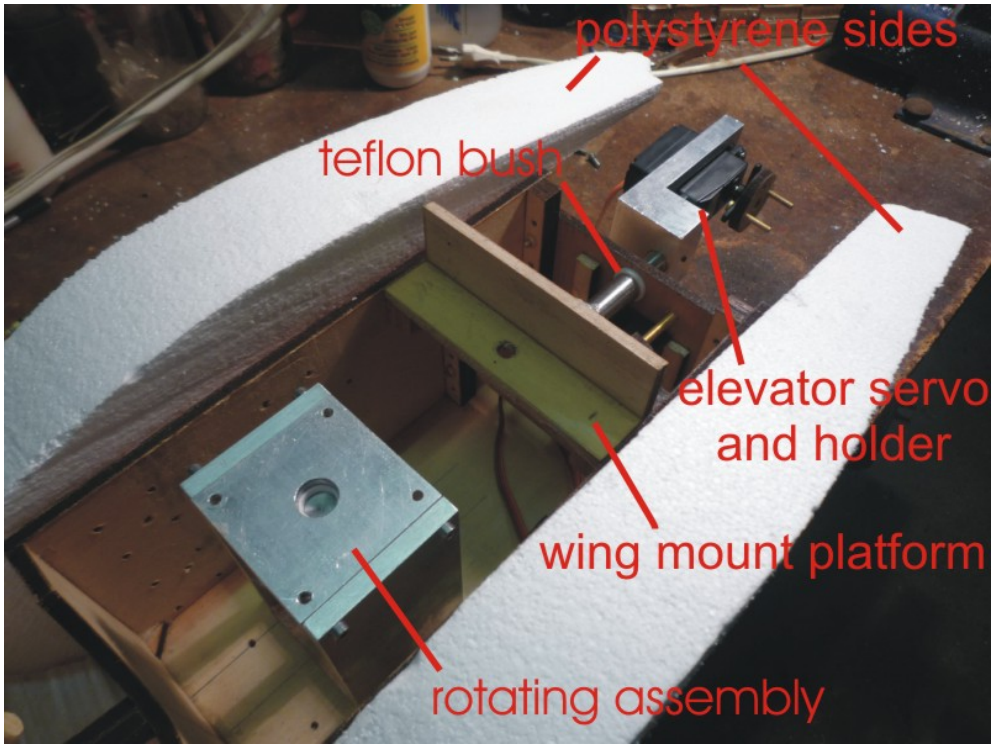

Figure 3.8: Oblique Top View of inside of finished Model

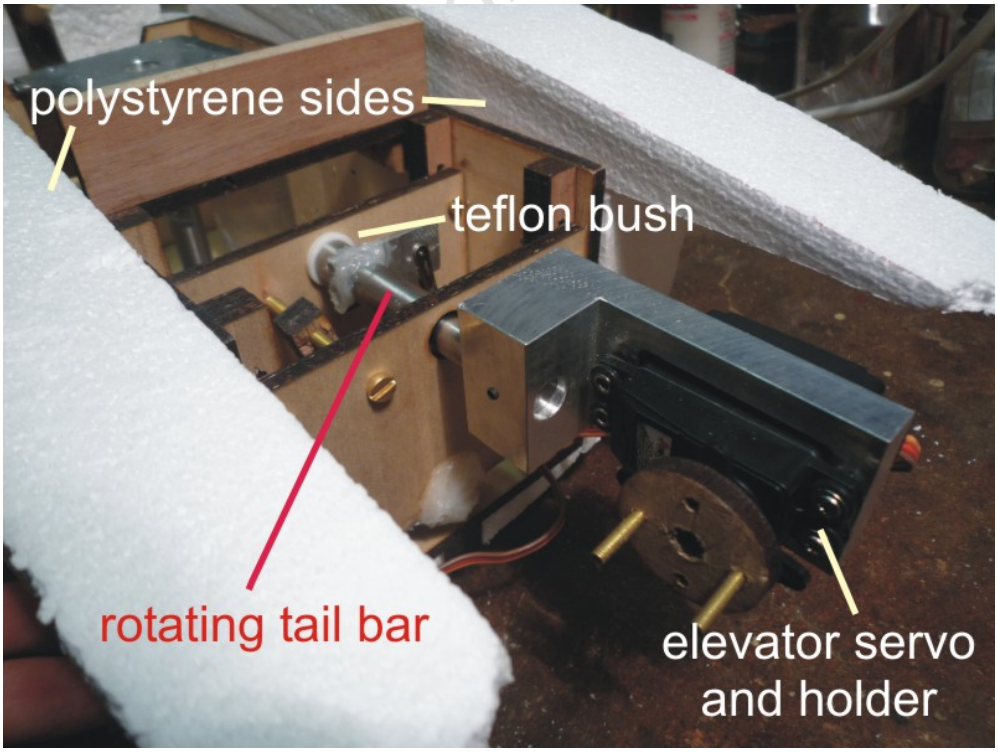

Figure 3.9: Oblique Back View of finished Model showing the Tail Control Section

3.4 Considerations with regard to the Dimensioning of the Model

3.4.1 The Airfoil

The airfoil of the Cape Vulture is unusual in many regards. There are thousands of airfoils available to choose from when designing a model aircraft (2227 in the particular edition of 'Profili' used [17]), but very few of them are comparable to that of the Cape Vulture (or any of the large soaring birds). The suggestion can be made that due to the sensory feedback mechanisms of the bird and the variable wing geometry, which includes changes in the airfoil [25], an airfoil that may be a bad choice for a model aircraft is a good choice for the bird. In general, an airfoil with a characteristic that deviates in a significant way from a particular average will limit a model to a particular flight regime, which is rarely desired.

With regard to the given experiment the only important factor is that the wing produces a similar downwash as compared to the real wing, since the downwash determines the local airflow that the tail flies in [38]. Characteristics such as lift and drag are unimportant in the context of this experiment. In general, it is thought of as bad practice to draw an airfoil 'by hand' and expect it to perform well when compared to computer-generated airfoils. For this experiment, however, an airfoil was drawn (the Cape Vulture Airfoil 'CVA') that quite simply and as accurately as possible followed the contours of the dissected Cape Vulture. It is depicted in figure 3.10.

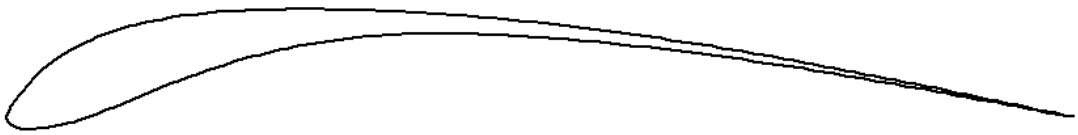

Figure 3.10: The Cape Vulture Airfoil 'CVA'

The airfoil was entered into the 'Profili' software and polars generated. These are shown in figure 3.11 and figure 3.12. The program encountered convergency problems when attempting to calculate certain regions of the polars for the CVA; these are missing from the polars.

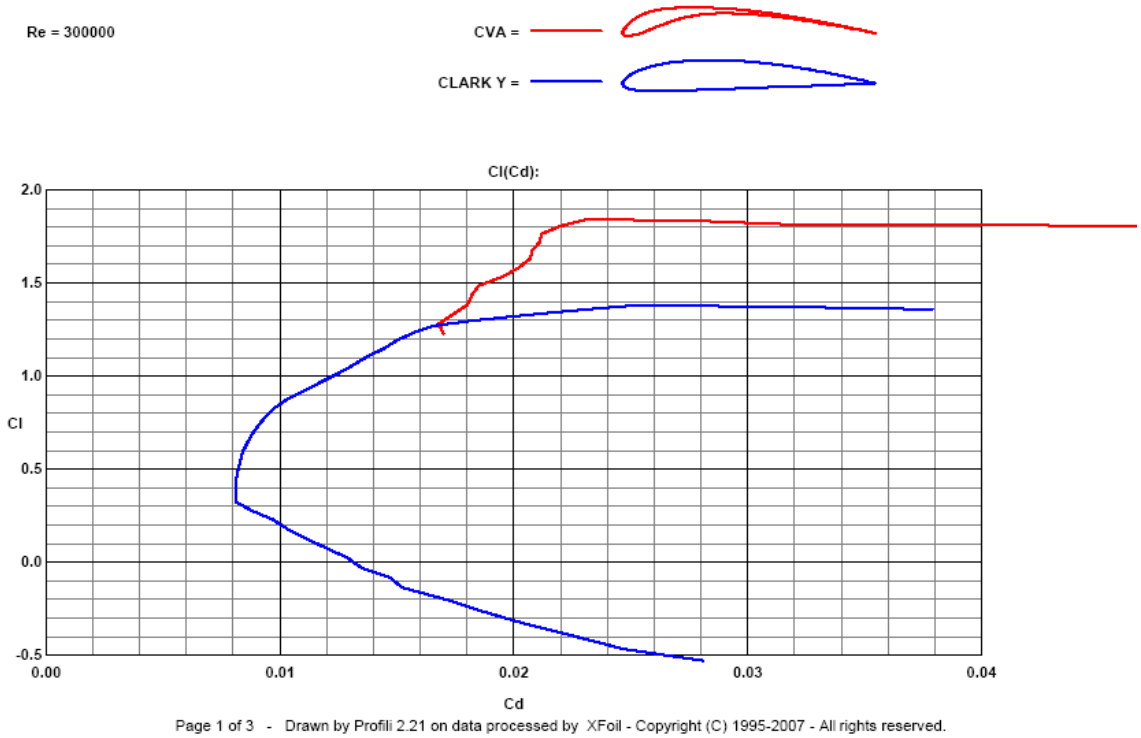

Figure 3.11: c_l vs. c_d Polar for the CVA

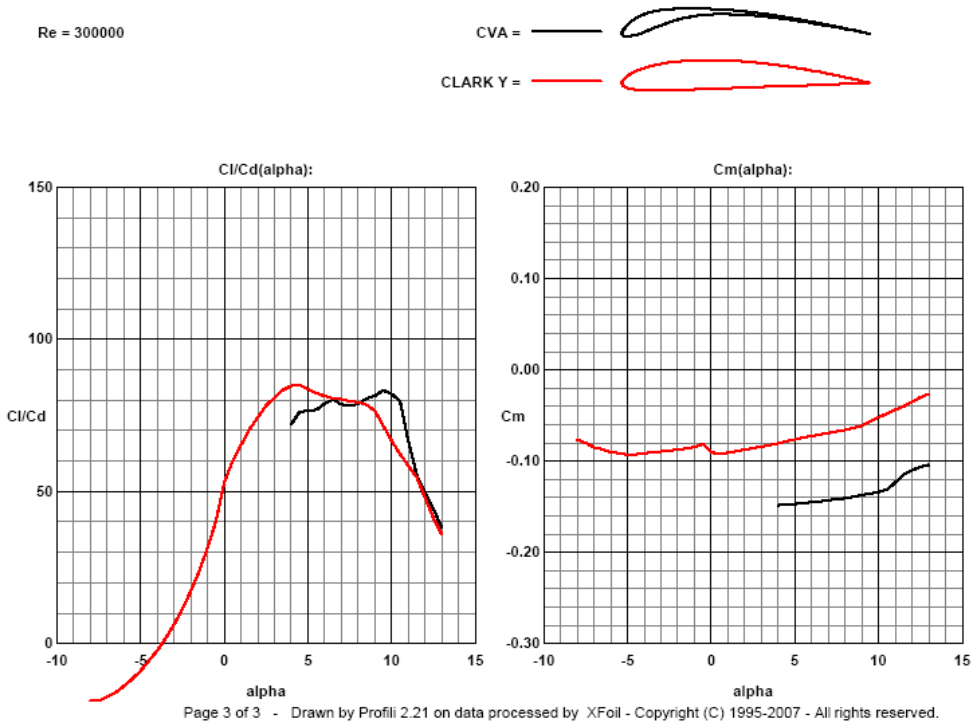

Figure 3.12: c_l / c_d vs. alpha Polar for the CVA

The polars predict better performance than what should have been hoped for from a hand-drawn airfoil. As would be expected from the large amount of camber, the maximum lift coefficient of the CVA is much higher than that of the Clark Y. The maximum c_l / c_d ratios are almost identical, with that of the Clark Y being in a safer area further away from the stall. This is more ideal for a model aircraft, but the maximum c_l / c_d ratio close to the stall is less of a problem for the bird with its feedback mechanisms and the ability to continually adjust the A.O.A. (even locally) according to current needs. Also, and again as would be expected from the large amount of camber, the negative pitching moment is larger for the CVA.

The distinguishing characteristics of the CVA are:

- Unusually high camber (see figure 3.13). The camber of the CVA is 9%, a very high value. Only 23 other airfoils of the 2227 available had a camber of over 8%.

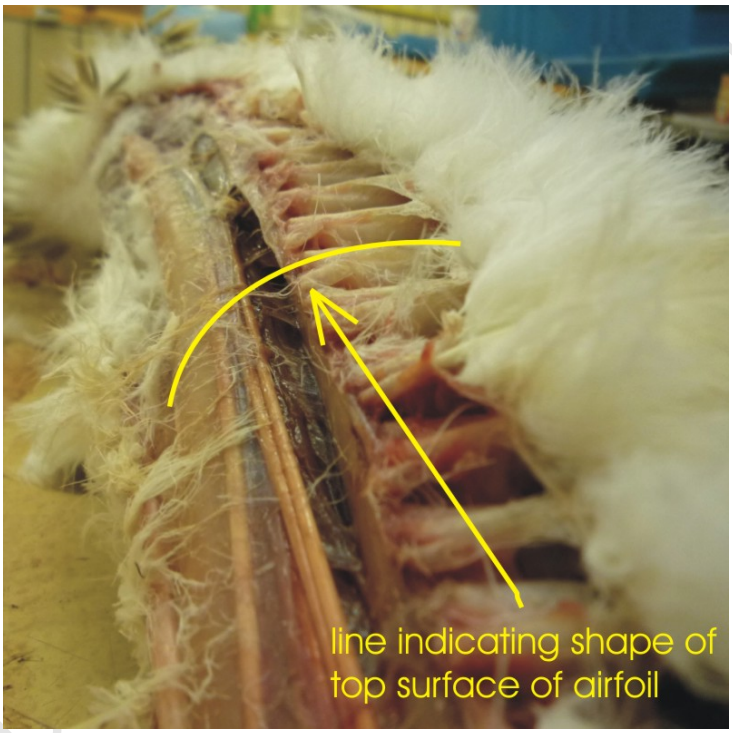

Figure 3.13: Figure indicating the large Amount of Camber in the front Section of the Airfoil

- The point of maximum thickness, lying at 10% of the chord, is unusually far forward. Only 11 other airfoils of the 2227 had their point of maximum thickness further forward than 15%. To investigate the effects of moving the point of maximum thickness two modified Clark Y airfoils were generated, Clark Y-mod1 with the point of maximum thickness moved forward 5% and Clark Y-mod2 with the point of maximum thickness moved back by 5%. The resulting polars are shown in figure 3.14 and figure 3.15. The Clark Y was chosen for this investigation since its characteristics are representative of a large range of airfoils.

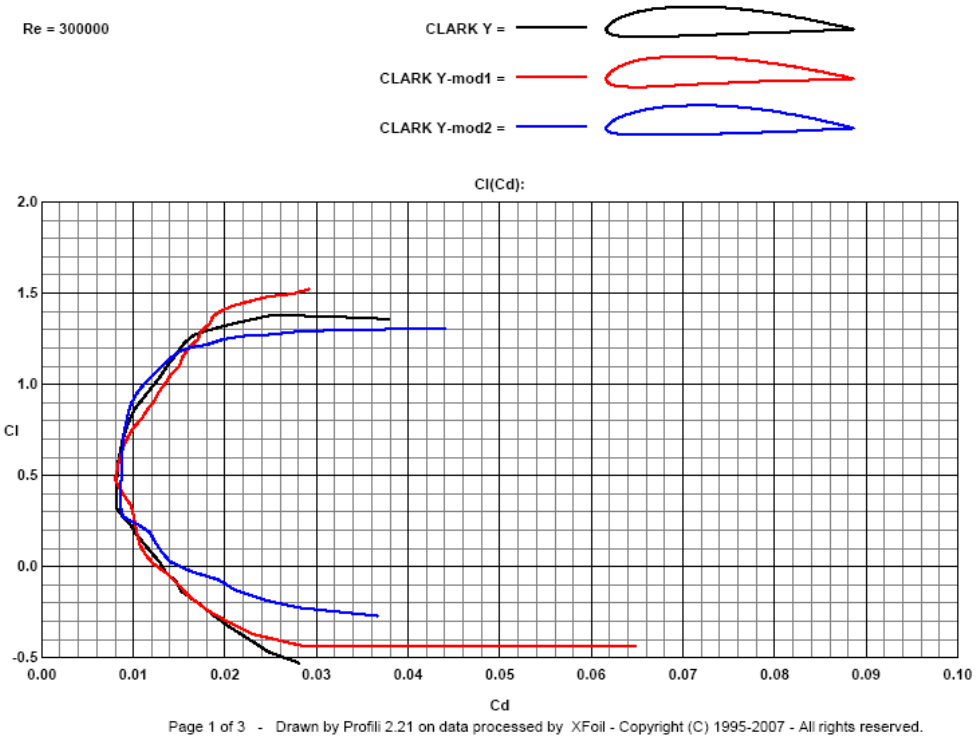

Figure 3.14: c_l vs. c_d Polars for original and modified Clark Y airfoils

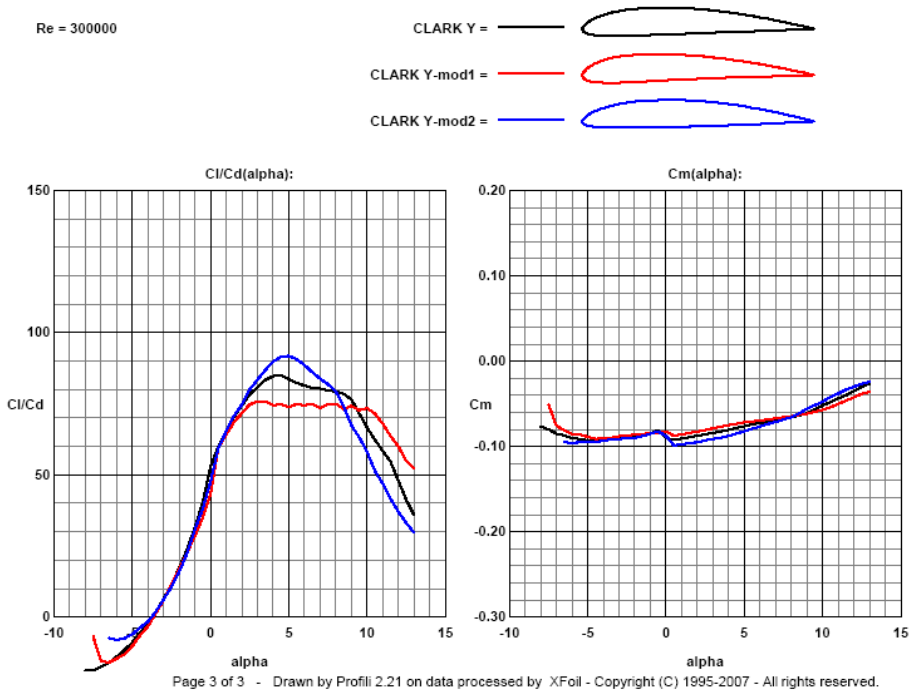

Figure 3.15: c_l / c_d and c_m vs. alpha Polars for original and modified Clark Y Airfoils

The c_l vs. c_d polar shows that moving the point of maximum thickness forward increases the maximum c_l attainable before the stall takes place. The c_l / c_d vs. alpha polar shows that moving the point of maximum thickness forward decreases the maximum c_l / c_d ratio but extends the usable range of A.O.A. Also the pitching moment becomes very slightly less negative.

- The thickness of the airfoil outside the region of the wing containing bones, muscles or patagia is literally no thicker than a feather, or two where they overlap. This pertains to the dark brown areas in figure 3.16, roughly two thirds of the wing. The CVA was given some thickness in this area to avoid constructional difficulties.

Figure 3.16: Figure indicating how much of the Wing Area is very thin

- The maximum thickness of the CVA, at 7.2%, would, according to the book Nurflügelmodelle [39], be incredibly low for the given wing loading of around 110g/dm^2. The recommended guideline for the thickness of an airfoil to be used is $\delta \approx 1.75 \times \sqrt{\frac{G}{F}}$, where δ is the recommended thickness and $\frac{G}{F}$ is the wing loading in g/dm^2. For a model aircraft with a wing loading of around 110 g/dm^2 this yields a thickness of around 18% for the airfoil, which deviates significantly from 7.2%. For a model aircraft the consequences of an excessively thin airfoil would be items such as a tendency to enter a spin when circling or to stall when coming in for the landing approach. There would also be constructional difficulties for the average modeller in creating a sufficiently strong and rigid wing.

3.4.2 Tail Placement

As stated in the previous section, the placement of the tail in relation to the wing is of some importance due to the downwash that the wing produces. Unfortunately, this fact was not yet realised at that point in time at which the dissection took place and no data was collected with regard to this item. However, figure 3.17 shows pictorial evidence that the tail is in a position slightly below the chord line of the wing.

Figure 3.17: Pictorial Evidence showing Position of the Tail in relation to the Wing [40] and [41]

This was observed in the construction of the model, figure 3.18 shows the side view of the tail area in SolidWorks. The black arrows indicate the vertical distance between the chord

lines of the wing and tail. The orange arrows indicate the horizontal position of the point of rotation being slightly forward of the T.E. A downward deflection thus simultaneously increases the vertical distance between the T.E. and the tail.

The author hypothesizes that this position of the tail slightly below the wing delays the stall for downward deflections of the tail in a similar way that raising the alula (the 'second finger' of a bird, refer to figure 2.1) delays the stall over the outer portion of the wing when the flying at high angles of attack (see figure 3.19). The alula achieves this by deflecting and compressing the airflow that would otherwise separate from the top surface of the wing onto the wing in such a way that the stall does not occur until the wing is at higher angles of attack than would otherwise be possible [42]. In a similar way, it is hypothesized, that part of the downwash that flows between the wing and the tail (indicated by the red line in figure 3.20) accelerates the airflow onto the top surface of the tail, thereby reducing flow separation and delaying the stall. Some commercial aircraft have 'alulas' in the form of leading edge slats.

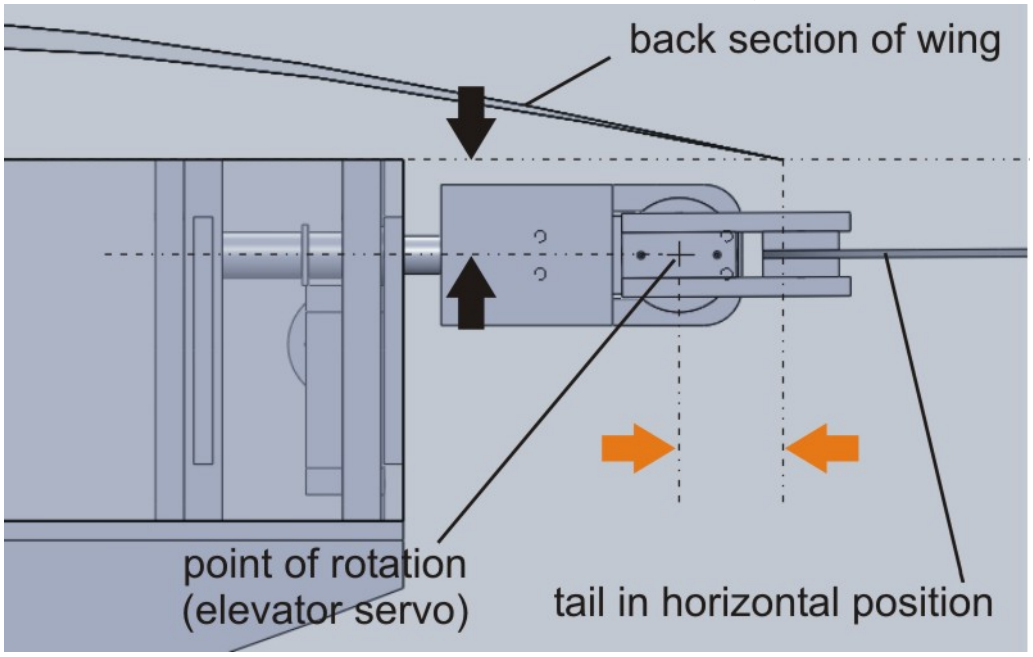

Figure 3.18: The Position of the Tail Unit in relation to the Wing

Figure 3.19: Raised Alulas deflecting Airflow

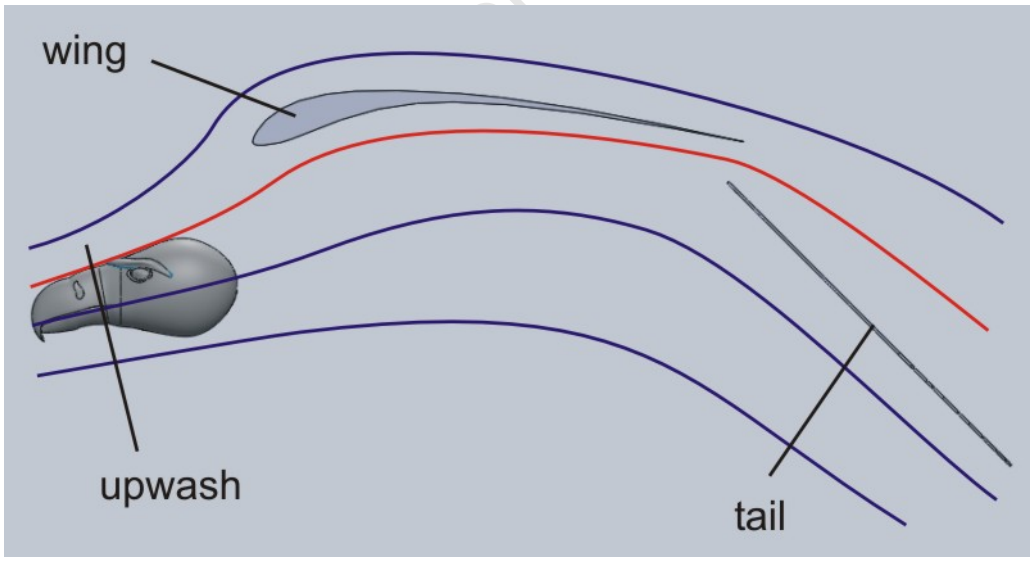

Figure 3.20: Hypothesised Airflow between Wing and Tail, Body not shown for Clarity

The tail unit was positioned based on the pictorial evidence. The result was a vertical distance of 24mm between the T.E. of the wing and the tail surface and a horizontal distance of 27.5mm between the T.E. of the wing and the point of rotation of the elevator servo.

3.4.3 Placement of Point of Rotation

Since the exact position of the C.G. was not known a choice needed to be made as to where the point around which the model would rotate would be placed. Even if this would have been thought of at the time of the dissection it would have been very difficult to determine since the body and wings would have to somehow be fixed in the position they have during flight or a piecewise reconstruction of the position of the C.G. would have had to be made. Accuracy would have been doubtful in the given context.

The point of rotation effectively emulates the position of the C.G. since an unconstricted body rotates about its C.G. The wing used in the model is simply a square wing. From the presented theory, the C.G. would need to be forward of 25% chord for stability. However as also already described, birds are not statically stable fliers and the C.G. lies aft of the 25% mark. Taking a lead from the Lelke experiments [29] in which a 28% chord C.G. position was achieved with the help of feedback (and limited by servos that turned out not to perform according to advertised speeds) and adding another small margin 30% chord was decided upon.

In terms of the vertical dimension an estimate was made taking into consideration the weight of the pectoral muscles and the total weight of the wings and assuming a constant density for the bulk of the body. Whether the stomach is full or empty would surely also affect the position of the C.G. to some degree. Rather than presenting numbers, the following SolidWorks image (figure 3.21) gives a good indication of the position that was decided upon.

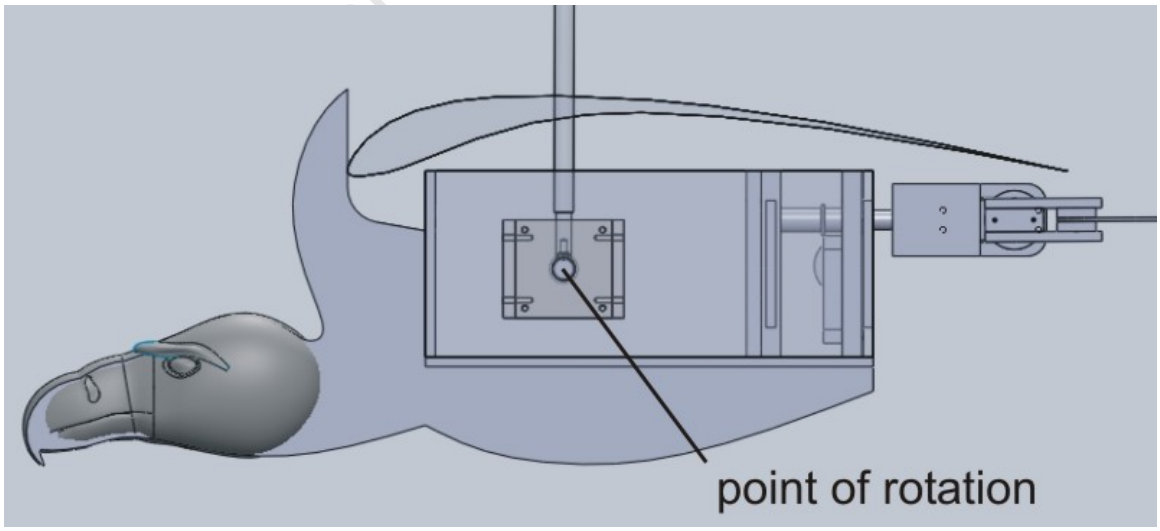

Figure 3.21: Indication of Point of Rotation for the Pitch Experiment

3.5 The Experimental Run

The experiment was conducted in the wind tunnel of the Department of Mechanical Engineering at the University of Cape Town. A picture of the complete wind tunnel is shown in figure 3.22 and a picture of the working area in figure 3.23, which shows the laptop used to control the servos, the power supply and the apparatus used to set and measure the airspeed in the wind tunnel. The mounted model is shown in figure 3.24.

Figure 3.22: Image of the Wind Tunnel in the Department of Mechanical Engineering at the University of Cape Town

Figure 3.23: Image of the Working Area

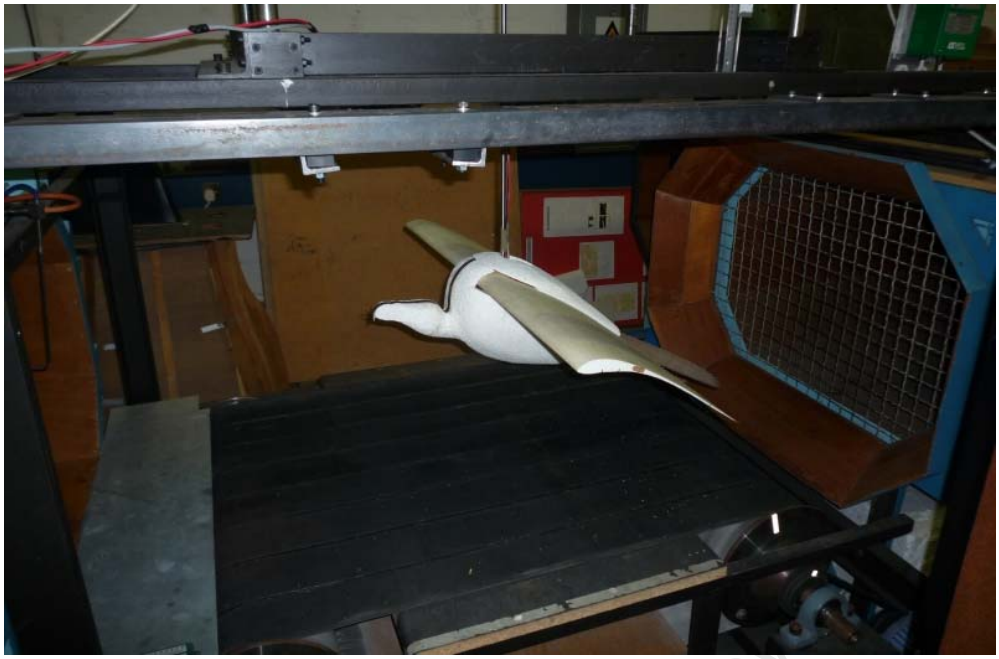

Figure 3.24: Model mounted in Wind Tunnel without Airflow

For this experiment the angle by which the pitch servo was deflected was defined as Φ. This is also the angle of incidence. A positive sign indicating a downward deflection of the tail (convention) and the angle through which the tail bar rotates be known as ξ, with a positive sign indicating a clockwise sense when viewed from behind (right hand rule). The red lines in figure 3.25 indicate the positive directions of these angles.

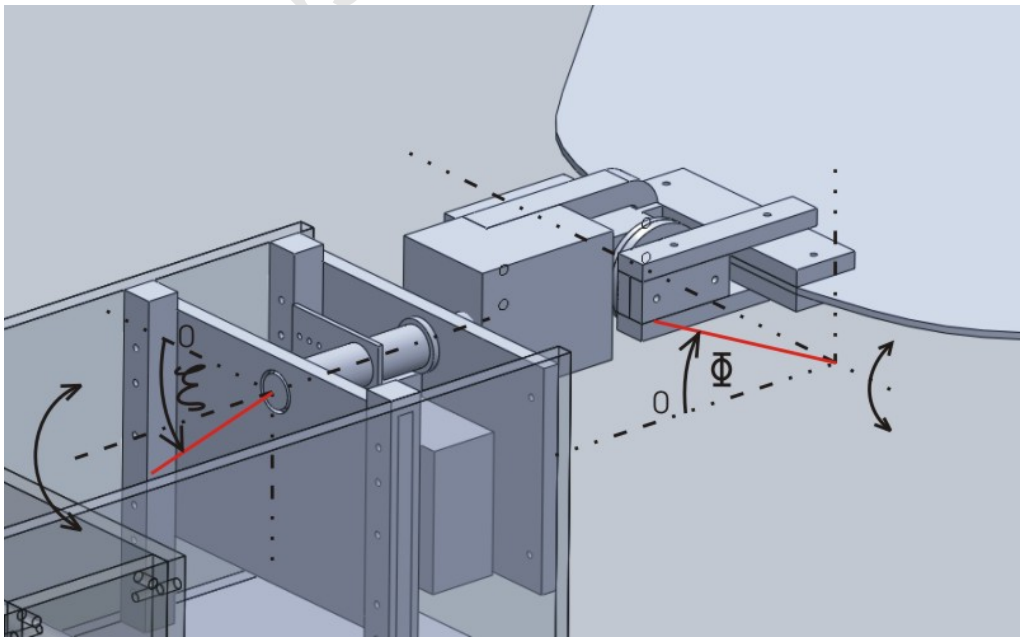

Figure 3.25: Clarification of Angles used in the Experiment

The apparatus with which the speed of the airflow in the wind tunnel is measured displays the airspeed in units of [km/h], hence the use of this unit. The SI unit [m/s] is given in brackets. The experimental sequence for measuring the torque generated about the pitch axis was to be as follows:

- Fix the model in the wind tunnel with the chord line of the wing horizontal and the tail in a horizontal position.
- Bring the speed of the airflow to 55 km/h (15.3 m/s, cruising speed of Cape Vulture 50-60km/h [43]).
- Set Φ and ξ to 0°.
- Measure the force required on the tip of the beak to keep the model in the neutral position.
- Repeat the measurement after incrementing Φ by 10°, up to a maximum value of 40°.
- Repeat the measurement set for negative values of Φ.
- Set ξ to 10°.
- Repeat the entire above measurement set.
- Repeat the entire above measurement set after incrementing ξ by 10°, up to a maximum value of 40°.

The experimental sequence for measuring the torque generated about the yaw and roll axes was to be similar except that only one side needed to be done due to symmetry.

From the measurements of the forces generated by such a representative set of tail positions it would then be possible to come to conclusions regarding the usefulness of the tail for stability and control of a bird robot.

The actual experiment ran a little different to the above plan, as follows:

To begin, the vulture model was mounted in the wind tunnel without the tail in such a manner that the degree of freedom was pitch. The actual C.G. is behind the point of rotation and the model thus the model tilted in a pitch up manner until mechanically constrained by the vertical bar coming up against the rotating assembly box, as shown in figure 3.24.

A downward force was applied to the beak to level out the model and the speed of the airflow was slowly incremented to become acquainted with the use of the wind tunnel. At an airspeed of 40 km/h (11.1 m/s) the model was beginning to shudder and risking a further increase seemed unreasonable. Also, the tail (still separate from the model) was held in the airstream and angled up and down and it became clear that the structure of the model would be put under an excessive strain from the forces so generated. In particular it was feared that

the assembly around the elevator servo might be overloaded since substantial torques would be generated around axes other than that normal to the servo output disk, although this remained to be seen.

For the next item the wind tunnel was switched off and the downward force on the beak required to keep the model level measured. This was repeated with increments in the airspeed of 10km/h (2.8 m/s), up to 40km/h (11.1 m/s). The results are shown in the figure 3.26.

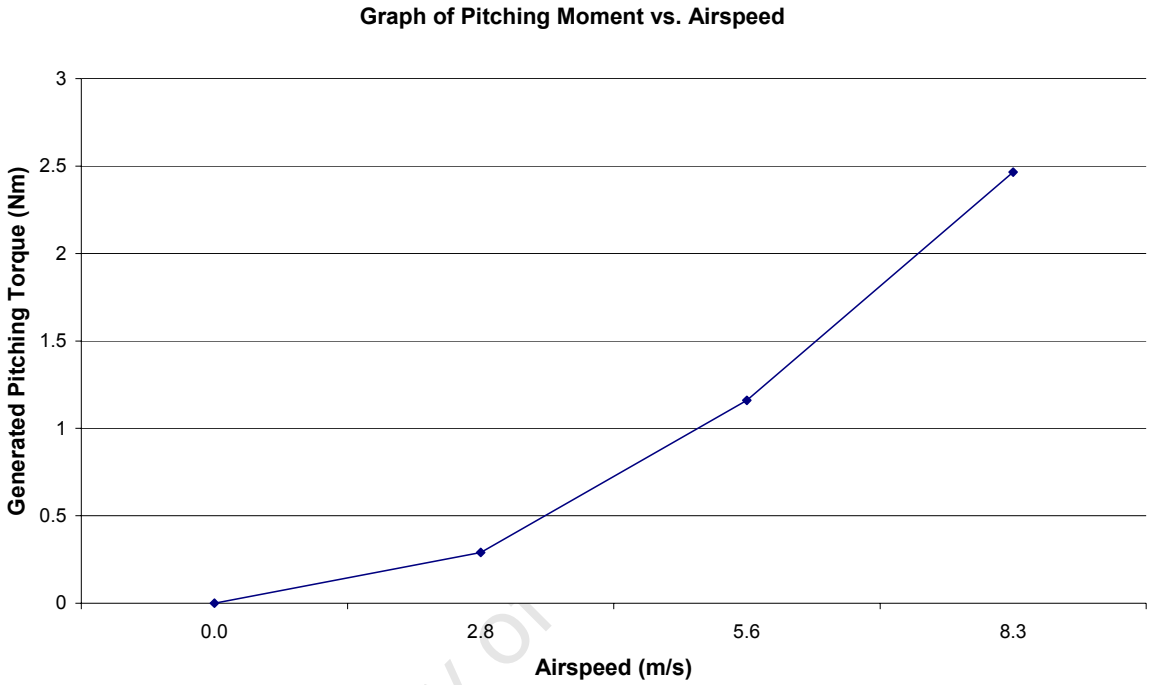

Figure 3.26: Graph showing Relationship between Airspeed and Pitching Moment

As the airspeed was brought up, the downward force required to keep the model level decreased. This was a convincing demonstration of the concept of negative pitching moment. The dependency of the force generated on the square of the airspeed is also very apparent in this experiment (see Eqn. 7).

Next the tail was held (by hand and still not physically attached to the body) in the position it would occupy if it was connected to the body, with a downward deflection of 45°. No downward force was applied to the beak. However, the model could be brought to a level position simply by deflecting the airflow behind it downwards (see figure 3.27). This is undoubtedly a variation of the 'ground effect' [44] wherein the lift force is increased when flying close to the ground since the high pressure region under the wing meets more resistance from the solid ground than it would from lower layers of air. Gulls, for example, make use of this effect when gliding along just above the water. In the case of the experiment, it is assumed that the lowered tail compresses the air in front of it, more so closer to the back of the wing than further forward. This results in a downward pitching moment, levelling out the model. This effect also affects birds when landing and they may be seen to stretch their wings particularly far forward when deflecting the tail down just before landing.

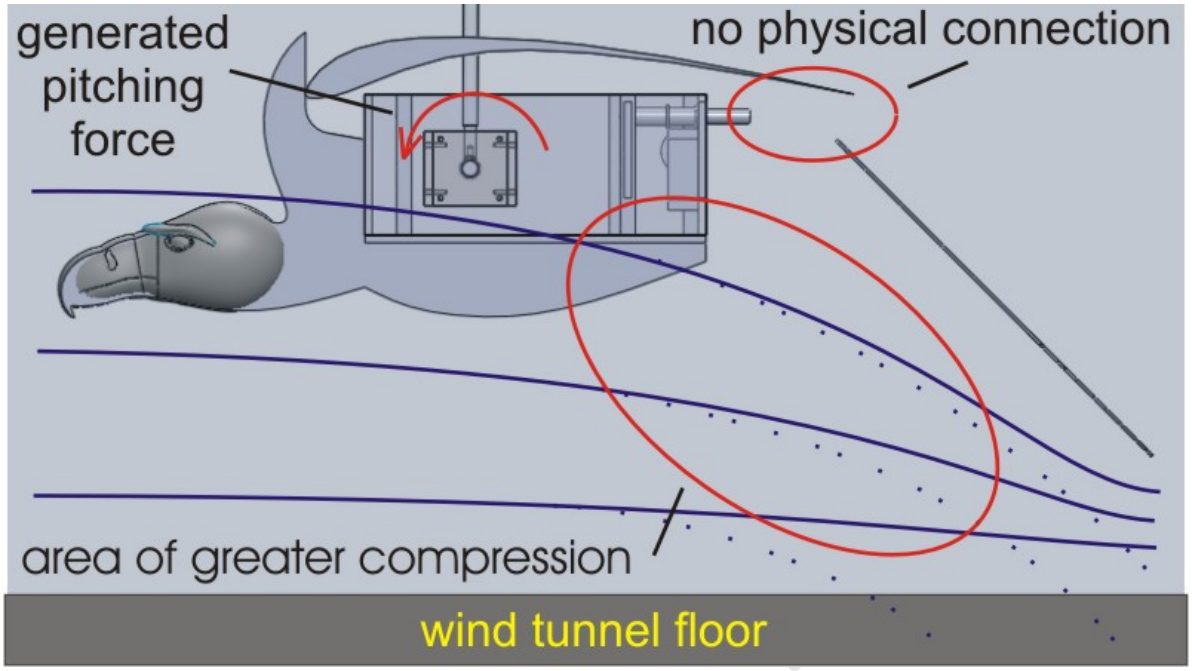

Figure 3.27: Effect of introducing the Tail, not connected to the Body, into the Airstream

In the figure the solid blue lines are an indication of the hypothesized airflow, with the narrow gap between the tail and the wind tunnel floor forcing a higher degree of air compression (the lines move closer together) than would otherwise be the case. For comparison, the dotted blue lines give an indication of what the airflow might have been like without the wind tunnel floor intervening (less compression). The figure is, of course, a simplification. Items such as span-wise flows and spillage around the side of the tail are not indicated.

Following this the tail was attached to the model and the experiments with regard to tail motion begun, starting with the pitch axis. All following experiments were run at an airspeed of 30km/h (8.3 m/s) for reasons already covered. Unfortunately results cannot be simply scaled up mathematically since the Reynolds number is also almost halved. Although this should be borne in mind, to the author the experiment is at least as much about 'what happens when' as it is about quantitative results.

The results for the degree of freedom of pitch are discussed referring to figure 3.28. These show the two extreme cases of roll servo deflections of 0° and 40°. The intermediate cases are merely transitionary examples and do not add to the discussion. The graphs shown take into consideration the measured pitching force at the airspeed of 30km/h (8.3 m/s) and isolate the effects of the tail, i.e. the data shows the torques generated by the tail alone.

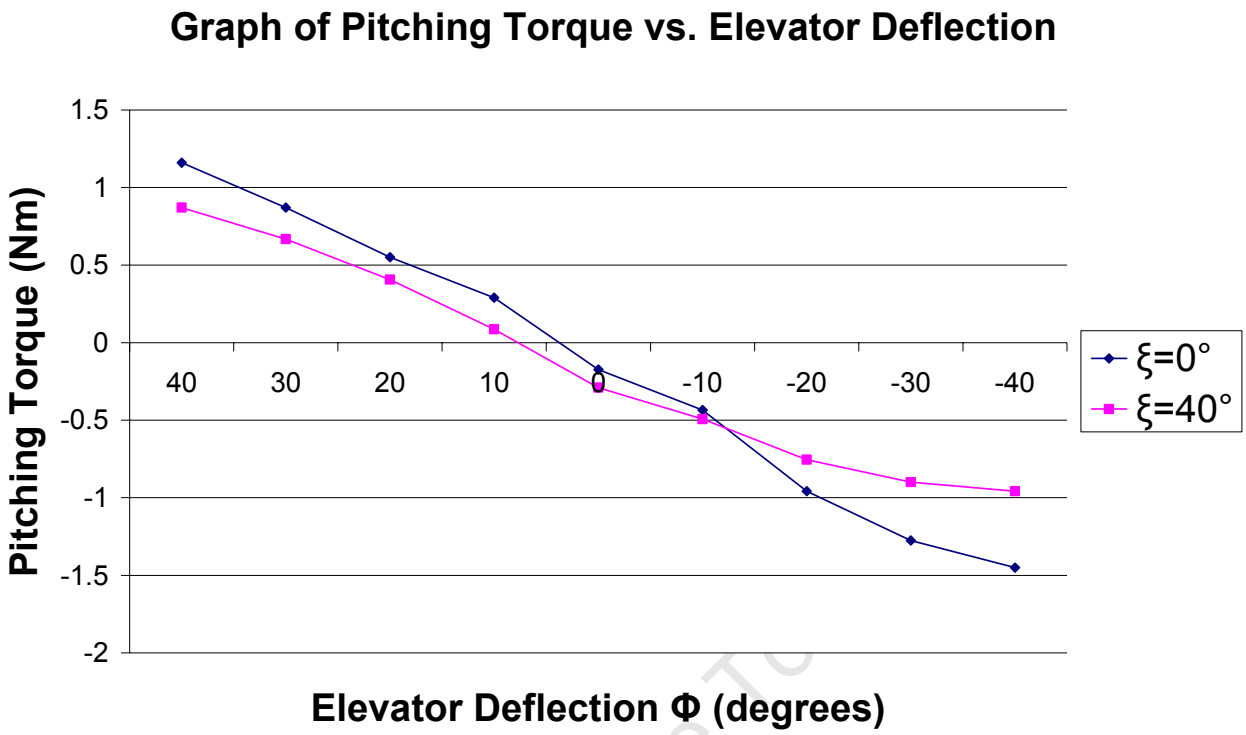

Figure 3.28: Graph showing Relationship between Pitching Force and Elevator Deflection for the Cases of no Roll Deflection and maximum roll Deflection

The distinguishing features in a comparison of the two curves are:

- A reduction of 30% in the difference between maximum torques for the case in which the roll servo is deflected
- The flattening of the curve at the extremes is more pronounced for negative elevator angles
- Both cases show a negative pitching torque for the case of zero elevator deflection

The first of these points seems obvious since as the roll angle ξ is increased the airflow is deflected increasingly sideways, thereby beginning to generate torque around other axes with a concomitant reduction in torque around the pitch axis.

The hypothesis for explaining the increased flattening of the curve for negative elevator angles as compared to positive elevator angles is twofold: Firstly, the ground effect may again be responsible for generating greater forces than would otherwise be created for positive elevator deflections, thereby contributing to re-linearising the curve in this region. Secondly, at the extreme of negative elevator deflection, the back portion of the tail begins to find itself in a region at the border of the airflow due to the dimensions of the wind tunnel. The vertical dimension of the airflow was not large compared to the model and placing the

model was a trade-off between ground effect and keeping all parts within the significant cross section of the airflow. Figure 3.29 gives an idea of the proportions involved. The vertical wooden stick in the foreground was used for reference marks.

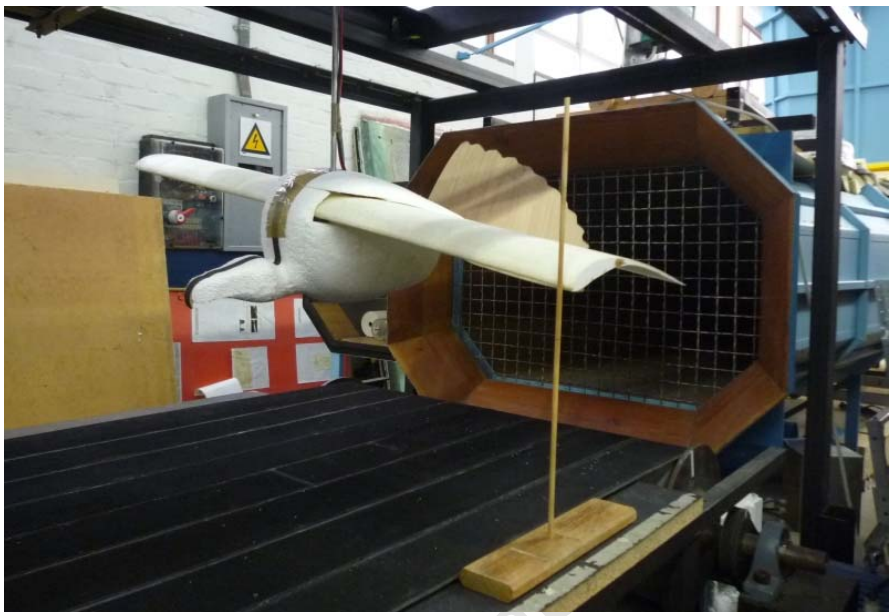

Figure 3.29: Figure showing Vertical Placement of Model in Wind Tunnel with back Region of Tail at Boundary of Airflow

The negative pitching torque for $\Phi = 0°$ comes about since the tail, when set at an angle of 0° relative to the wing, is operating at a negative A.O.A. due to the downwash behind the wing. In soaring flight the angle of incidence may thus be seen to be slightly negative, as indicated in figure 3.30. This is in stark contrast to a conventional aircraft configuration.

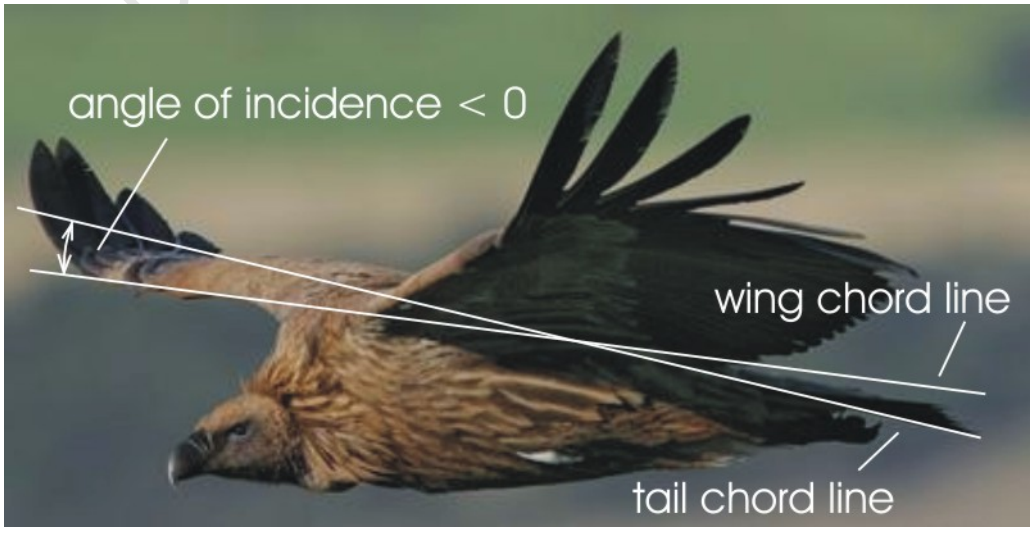

Figure 3.30: Indication of Angle of Incidence in Soaring Flight

It would have been expected that the pitching torque at $\Phi = 0°$ for the case $\xi = 0°$ would be more negative than that for the case $\xi = 40°$. Inaccuracies in the measurement apparatus, consisting of spring balances, were considered and another measurement taken for $\Phi = 0°$ and $\xi = 0°$. This measurement did, in fact, indicate a more negative pitching torque (by about 0.15Nm) for the case $\xi = 0°$ than for the case $\xi = 40°$. This is not indicated on the graph since it was not possible to include a single additional measurement point.

This also shows that in the given context the tendencies of the results, rather than the value of a particular data point, should be looked at.

The model was then taken apart, rebuilt and remounted with the degree of freedom now being the roll axis. The forces generated were too small to be effectively measured with the available spring balances. With the tail in the extreme positions, a tendency to roll one way or the other could be seen as per the following:

- Elevator full positive, roll full positive → negative roll
- Elevator full positive, roll full negative → positive roll
- Elevator full negative, roll full positive → positive roll
- Elevator full negative, roll full negative → negative roll (see figure 3.29).

As noted before these were tendencies at best, however they were repeatable and the initial position of the model was irrelevant.

The model was then set up for measurements in the yaw axis. The first item to note was that with the tail in a neutral position the model displayed negative weathercock stability. After the head was placed in the centre the model would yaw one way or the other. Interestingly, as some elevator deflection was introduced stability arose; 10° of deflection were sufficient. The model could be pushed off-centre and was found to return to centre. For a discussion of the quantitative results figure 3.31 may be referred to.

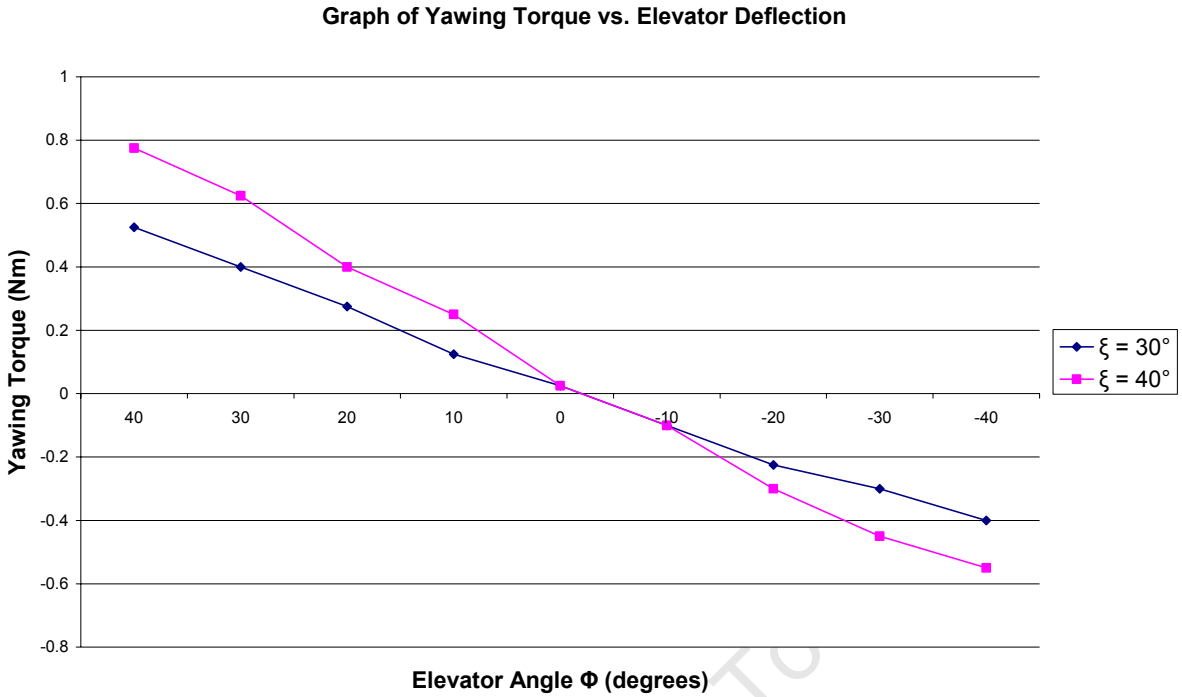

Figure 3.31: Graph showing Relationship between Yawing Torque and Elevator Deflection with Roll Deflections of 30° and 40°

Features of these two curves are:

- Greater magnitude of torque for positive deflections as compared to negative deflections
- A slight flattening of the curve for the larger negative elevator deflections that is not reflected in the positive deflections

These effects could be contributed to by the ground effect and the placement of the model in the airstream, as previously discussed. The curve for $\xi = 30°$, which has essentially the same shape as that for $\xi = 40°$, was included only to show that the flattening of the curve for negative elevator deflections was not a statistical deviation of one particular measurement set.

To finish off the model was tethered so that it was constrained to yaw to a maximum of about 45° either way. The elevator was set to maximum positive deflection and the roll servo then moved from one extreme to the other. The rather marked effect that this had on the orientation of the model may be observed by watching the movie clip available at http://www.youtube.com/watch?v=r6BV6TRAMjE.

3.6 Chapter Conclusion

The experiment on whole yielded no surprises. It was, however, very interesting to observe the theory in action. The experiment showed that the Cape Vulture is certainly very capable of producing, with its tail, strong pitching forces, somewhat weaker but still very effective (as may be seen in the movie clip) yawing forces but almost no rolling force. Also, additional pitching forces need to be reckoned with when flying close to the ground. Despite all of this, it must be borne in mind that the tail would hardly move in soaring flight but only moves significantly when maneuvering, such as when coming in to land (see figure 3.32). City pigeons that have to change direction frequently in flight may be observed to use their tails much more than large soaring birds. It must also not be forgotten that the wings are used in conjunction with the tail to change the flight path. This experiment looked at the tail only.

Figure 3.32: Landing Cape Vulture [45]

4 Conclusions

Certainly many of the challenges involved in the construction of a flying bird robot have been uncovered and some of them looked at in greater detail. It may conclusively be said that creating such a robot is an elusive task, as evidenced by the large number of partial and incomplete solutions.

As yet there seems to be no solution that satisfactorily emulates the functions of the wing of a real bird with regard to flight dynamics. In looking at previous projects by others, the quetzalcoatlus model is the only one that implemented pitch control by movement of the A.C. All other models that were looked at resort to the use of hinged surfaces for control in one or more of the three axes. Also, and importantly, with regard to the pitch axis there seems to be no alternative to active control with feedback if airfoil performance is not to be sacrificed.

The experiment has shown, not surprisingly, that the tail is capable of generating sufficient force around the pitch axis for it to be included in a pitch control scheme.

Similar conclusions apply to control of the yaw axis. Again the quetzalcoatlus model is the only one that used active control with feedback, with this particular animal having the advantage of a large vertical surface (the head and beak) through which to effect the control. Aside from the 'Milan' model which forces yaw stability through its design but is unable to generate a controlled force around the yaw axis, all other projects looked at needed to in some way artificially create a sufficiently large amount of vertical surface for stability and in some cases control.

The experiment has shown that the tail is definitely capable of producing sufficient force for control around the yaw axis if given sufficient degrees of freedom to do so. However, since the tail would not be turned to be entirely vertical and generating a force around the yaw axis simultaneously generates a force around the pitch axis other compensatory control elements would need to be involved as well to implement yaw control through the use of the tail. However, it seems that with a sufficiently complex control scheme vertical surfaces as such could be completely eliminated without sacrificing stability or control around the yaw axis.

Although control in the roll axis is desired, the roll axis is that axis in which stability is least problematic since the natural position of the wings ensures it while soaring. The experimental result that the tail is not very effective in generating forces around the roll axis does thus not seem detrimental. In fact, it would probably simplify the control scheme since the effect of tail movements on roll would hardly have to be considered, with roll control then being left to the wing.

Also, the experiment has shown that a control scheme would have to be capable of dealing with the additional forces created by the ground effect to cater for additional pitching forces when flying close to the ground, such as when landing.

Although not recommendable for most model aircraft applications, the CVA airfoil was considered to be successful in this context.

5 Recommendations

Clearly the accuracy of the results with regard to how well they represent the real-life scenario of the flying vulture depends on the accuracy of the model and of the measuring equipment.

The three dimensional shape of the model is regarded as being fairly accurate, being directly based on the dissected Cape Vulture. Also the slightly rough surface texture is thought of as being very close to the original 'feather' texture in terms of airflow over it.

The motion of the tail could be improved upon. When the tail is moved in the roll axis, by symmetry one side of the tail moves up as much as the other moves down whereas a real bird moves the axis of rotation towards the up-going side and down for most manoeuvres to decrease the amount by which the tail moves on that side. This would, however, have been quite difficult to implement mechanically in the model.

The sizing of the model should definitely have been considered in more detail before commencing design and construction. At the outset, it was not certain in which wind tunnel the experiment would be conducted. The intention behind creating a life-size model was to approximate the flight conditions of the Cape Vulture as closely as possible. However, with the relatively small size of the wind tunnel forcing some degree of ground effect and the tail moving into the cross-sectional boundary of the airstream a smaller model may well have been a better choice. A smaller model may also have allowed the experiment to be run at a higher airspeed, possibly moving the experiment into a region of Reynolds number that is closer to that at which the real vulture flies.

As shown in the previous chapter, the tail is an obvious and very capable candidate for inclusion in any control scheme. For a control scheme that approaches that of the real bird, however, it seems impossible not to include the effects of the wing on control as well. The interaction of the wing and the tail, in particular with regard to the pitch and yaw axes, would need further investigation. Since the wings are the main pitch control device when in soaring flight it would be interesting to investigate for which flight situations it becomes beneficial to involve the tail. As for the yaw axis, as shown in the previous chapter, wing involvement is forced when using the tail and it would be interesting to investigate how the wing would be involved in yaw control.

In any further development of the model it would also seem beneficial not to deviate from the CVA in any significant way without consideration of the consequences that this would imply.

6 References

1. *The World Book Encyclopedia, Volume 5*. Chicago: World Books, 1987, pg. 2.
2. *The World Book Encyclopedia, Volume 21*. Chicago: World Books, pp. 420-422.
3. Bill and Bunny Kuhlmann. "Twist Distributions for Swept Wings, Part 1". Internet: http://www.rcsoaringdigest.com/OTW/on-the-wing4/161-HCP1.pdf, [Dec. 2, 2010].
4. Karl Herzog."Der Schwingenflug in der Natur und in der Technik". *Mechanikus*, page 20, Feb. 1963.
5. Martin Simons. *Model Aircraft Aerodynamics*. Herts: Argus Books, 1994.
6. Ira H. Abbott and Albert E. von Doenhoff. *Theory of Wing Sections*. New York: Dover Publications, 1959, pp. 112-113.
7. Jeff Scott. "Lift & Drag vs. Normal & Axial Force". Internet: http://www.aerospaceweb.org/question/aerodynamics/q0194.shtml, [Dec. 2, 2010].
8. Paul Gladman. "Smoke Angel". Internet: www.flightglobal.com/blogs/aircraft-pictures/2008/08/smoke-angel.html, [Dec. 2, 2010].
9. Phillip Burgers. "Does a Bird have a Tail to tell?". Internet: http://www.rcsoaringdigest.com/OTW/on-the-wing3/Do_birds_have_tails.pdf, [Dec. 2, 2010]
10. Gottfried Sachs. "Effect of slotted wingtips on yawing moment characteristics". *Journal of Theoretical Biology*, vol. 239, pp.93–100, 2006.
11. Gottfried Sachs. "Aerodynamic yawing moment characteristics of bird wings". *Journal of Theoretical Biology*, vol. 234, pp. 471–478, 2005.
12. Gottfried Sachs. "Tail effects on yaw stability in birds". *Journal of Theoretical Biology*, vol. 249, pp. 464–472, 2007.
13. J. Page and E.S. Morton. *Lords Of The Air*. Washington, DC: Smithsonian Books, 1995, found referenced at http://www.twitt.org/SydHall.html, [Nov. 24, 2010].
14. Internet: http://www.twitt.org/OSHKCO4.xls, [Nov. 24, 2010].
15. "Bob Hoey's "Birds" Part 1". Internet: http://www.twitt.org/1partdrib.html, [Nov. 24, 2010].
16. Jack Edwards. "Eddie the Eagle". *Silent Flight*, pp.26-29, Feb./Mar. 1993.

17. Stefano Duranti. Internet: http://www.profili2.com, [Dec. 2, 2010].

18. Franz Klement. "RC-Möwe Emma". *Flug- und Modelltechnik*, vol. 393, pp.20-24, Oct. 1988.

19. Paul Pursglove. "Discovering Pterosaur flight - Part 2". Internet: http://pterodata.blogspot.com/2009_06_01_archive.html, Jun.15 2009 [Dec. 2, 2010].

20. Stephen Winkworth. "Pteranodon IV". *RCM&E Plans Service*, RC1583.

21. Bill and Bunny Kuhlmann. "Twist Distributions for Swept Wings, Part 3". Internet: http://www.rcsoaringdigest.com/OTW/on-the-wing4/163-HCP3.pdf, [Dec. 2, 2010].

22. Philippe Ballarini. "Two brothers, one wing". Internet: http://aerostories.free.fr/constructeurs/horten/page2.html, [Nov. 24, 2010]

23. Internet: http://das-nurfluegelteam.de/, click on Software "Laschka", [Dec. 2, 2010].

24. Internet: http://www.zanonia.de/ranis.php, [Dec. 2, 2010].

25. Robert Schweissgut. Internet: http://www.flying-wing.de/rs/katalog/rs_milan.html, [Dec. 2, 2010].

26. Reinhard Weber. "Der Beweis, daß die Riesensaurier fliegen konnten". *P.M. Magazin*, pp.76-84, Jun. 1985.

27. Hans-Jürgen Raabe. "Flug in die Urzeit". *Bunte*, pg.62, May 1986.

28. Henry Jex. "Making Pterodactyls Fly". Internet: www.twitt.org/QNStory.html, [Dec. 2, 2010].

29. Helmut Lelke. "Airfoil Performance Concepts". Internet: www.charlesriverrc.org/articles/asfwpp/lelke_airfoilperf.htm, [Dec. 2, 2010].

30. Helmut Lelke. "Active Pitch Stabilizer Concept". Internet: http://www.charlesriverrc.org/articles/asfwpp/lelke_activepitch.htm, [Dec. 2, 2010].

31. Internet: http://ovirc.free.fr/McCready.php, video material, [Dec. 2, 2010].

32. Internet: http://www.photographersdirect.com/buyers/stockphoto.asp?imageid=492151, [Dec. 2, 2010].

33. Terry Andrews. Internet: http://www.panoramio.com/photo/6767862, [Dec. 2, 2010].

34. Internet: http://www.photographersdirect.com/buyers/stockphoto.asp?imageid=1070209, [Dec.2 , 2010].

35. Matthew Naylor. "Hare - Eagles Dare". Internet: http://www.fwi.co.uk/blogs/lincolnshire-farming-blog/2008/11/hare-eagles-dare.html, Nov.22, 2008 [Dec. 2, 2010].

36. Bill and Bunny Kuhlman. "Inhibiting Flutter" in *On the Wing*. Seattle, Washington: B^2Streamlines, 1995, pp.148-153. Also available at http://www.rcsoaringdigest.com/OTW/on-the-wing1/33InhibitingFlutter.pdf

37. Internet: http://www.photographersdirect.com/buyers/stockphoto.asp?imageid=2716591, [Dec. 2, 2010].

38. Bill and Bunny Kuhlmann. "Twist Distributions for Swept Wings, Part 2". Internet: http://www.rcsoaringdigest.com/OTW/on-the-wing4/162-HCP2.pdf, [Dec. 2, 2010].

39. Dipl.-Ing. Martin Lichte. *Nurflügelmodelle*. Baden-Baden: Verlag für Technik und Handwerk, 1987, pg. 31.

40. Internet: http://www.flickr.com/photos/wildimages/107543628/, [Dec. 2, 2010].

41. Internet: http://www.wildlife-expressions.co.za/images/phocagallery/Cape%20Vulture/thumbs/phoca_thumb_l_cape-vulture.jpg, [Dec. 2, 2010].

42. K. Simkiss. *Bird Flight*. London: Hutchinson Educational, 1963, pp.34-36.

43. Dr. Robert Simmons, *pers. comm.*

44. Heinrich Völker. "Die Sache mit dem Bodeneffekt". *Flug- und Modelltechnik*, vol. 491, pp.14-17, Dec. 1996.

45. Andre Botha. Internet: http://www.vultureday.org/wp/wp-content/gallery/africa/cape-vulture_imm_kempenfeldt-kzn_3-7-09-1.jpg, [Dec. 2, 2010].

Appendix A

Equations

$$L = \frac{1}{2}\rho V^2 S C_L, \qquad \text{(Eqn. 1)}$$

where L is the lift force, ρ the air density, V the velocity, S the surface area, and C_L the lift coefficient.

$$D = \frac{1}{2}\rho V^2 S C_D, \qquad \text{(Eqn. 2)}$$

where D is the drag force and C_D the drag coefficient.

$$\mathrm{Re} = \frac{\rho V L}{\mu}, \qquad \text{(Eqn. 3)}$$

where Re is the Reynolds number, L is the length (wing chord in these discussions), and μ is the viscosity.

$$A = \frac{b^2}{S}, \qquad \text{(Eqn. 4)}$$

where A is the aspect ratio, and b is the span.

$$C_{Di} = k \times \frac{C_L^{\,2}}{\pi \times A}, \qquad \text{(Eqn. 5)}$$

where k is a factor to allow for deviations from the ideal elliptical lift distribution.

$$\delta \approx 1.75 \times \sqrt{\frac{G}{F}}, \qquad \text{(Eqn. 6)}$$

where δ is the recommended thickness of the airfoil and $\frac{G}{F}$ is the wing loading in g/dm^2.

$$M = \frac{1}{2}\rho V^2 S c c_{mo}, \qquad \text{(Eqn. 7)}$$

where M is the pitching moment, c the chord and c_{mo} the pitching moment coefficient.